Final Technical Report on FA2386-10-1-4100 (AOARD-104110)

Epitaxial growths of *m*-plane AlGaN/GaN and AlInN/GaN heterostructures applicable for normally-off mode high power field effect transistors on freestanding GaN substrates

Principal Investigator:
Shigefusa F. Chichibu, Dr. Eng. (Professor)
Tohoku University
Center for Advanced Nitride Technology (CANTech)
Institute of Multidisciplinary Research for Advanced Materials (IMRAM)
2-1-1 Katahira, Aoba, Sendai 980-8577, Japan
Area Code/Phone Number: +81-22-217-5360 Fax Number: +81-22-217-5360
E-mail: chichibu@tagen.tohoku.ac.jp
Co-Principal Investigators:
Kouji Hazu, Dr. Eng. (Assistant Professor, Chichibu Lab., Tohoku University)
E-mail: k_hazu@tagen.tohoku.ac.jp

Contents

A Statement of Work Approved

B Milestones and Deliverables Originally Planned

C Summary of the results (15 Apr. 2010 - 14 Aug. 2011 - approved Earthquake delay)
(0) Overview
(1) Polarization properties of *m*-plane $Al_xGa_{1-x}N$ films grown by MOVPE and NH_3-MBE on MCC *m*-plane free-standing GaN substrates
(2) Impacts of anisotropic tilt mosaics of state-of-the-art *m*-plane freestanding GaN substrates on the structural and luminescent properties of *m*-plane $Al_xGa_{1-x}N$ epilayers
(3) MOVPE and characterization of *m*-plane $Al_{1-x}In_xN$ films on the freestanding GaN substrates
(4) MOVPE and characterization of AlGaN / GaN and AlInN / GaN heterostructures

D Technical Reports
(1) Polarization properties of *m*-plane $Al_xGa_{1-x}N$ films grown by MOVPE and NH_3-MBE on MCC *m*-plane free-standing GaN substrates
(2) Impacts of anisotropic tilt mosaics of state-of-the-art *m*-plane freestanding GaN substrates on the structural and luminescent properties of *m*-plane $Al_xGa_{1-x}N$ epilayers
(3) MOVPE and characterization of *m*-plane $Al_{1-x}In_xN$ films on the freestanding GaN substrates
(4) MOVPE and characterization of AlGaN / GaN and AlInN / GaN heterostructures

Report Documentation Page

Form Approved
OMB No. 0704-0188

1. REPORT DATE	2. REPORT TYPE	3. DATES COVERED
17 AUG 2011		

4. TITLE AND SUBTITLE	5a. CONTRACT NUMBER
Epitaxial growths of m-plane AlGaN/GaN and AlInN/GaN heterostructures applicable for normally-off mode high power field effect transistors on freestanding GaN substrates	**FA23861014100**
	5b. GRANT NUMBER
	5c. PROGRAM ELEMENT NUMBER

6. AUTHOR(S)	5d. PROJECT NUMBER
Shigefusa Chichibu	5e. TASK NUMBER
	5f. WORK UNIT NUMBER

7. PERFORMING ORGANIZATION NAME(S) AND ADDRESS(ES)	8. PERFORMING ORGANIZATION REPORT NUMBER
Tohoku University, Institute of Multidisciplinary Research for Advanced Material,2-1-1 Katahira,Aoba, Sendai,Miyagi 980-8577,JP,980-8577	**N/A**

9. SPONSORING/MONITORING AGENCY NAME(S) AND ADDRESS(ES)	10. SPONSOR/MONITOR'S ACRONYM(S)
	11. SPONSOR/MONITOR'S REPORT NUMBER(S)

12. DISTRIBUTION/AVAILABILITY STATEMENT

Approved for public release; distribution unlimited.

13. SUPPLEMENTARY NOTES

14. ABSTRACT

Non-polar m-plane AlxGa1-xN and Al1-xInxN alloy films and heterostructures were grown by metalorganic vapor phase epitaxy (MOVPE) in order to obtain fundamental understandings on the growth of m-plane nitrides and carrier transport mechanisms. These alloys are being investigated for potential use in normally-off heterojunction field effect transistors (HFETs).

15. SUBJECT TERMS

16. SECURITY CLASSIFICATION OF:			17. LIMITATION OF ABSTRACT	18. NUMBER OF PAGES	19a. NAME OF RESPONSIBLE PERSON
a. REPORT	b. ABSTRACT	c. THIS PAGE			
unclassified	**unclassified**	**unclassified**		**32**	

A Statement of the Work Approved for FA2386-10-1-4100

Abstract:

We are going to grow nonpolar *m*-plane $Al_xGa_{1-x}N$ and $Al_{1-x}In_xN$ alloy films and heterostructures by metalorganic vapor phase epitaxy (MOVPE), in order to obtain fundamental understandings on the growth of *m*-plane nitrides and carrier transport mechanisms. Those alloys are one of the possible candidates for the fabrication of normally-off heterojunction field effect transistors (HFETs).

Objectives:

1. Grow nonpolar *m*-plane $Al_xGa_{1-x}N$ and $Al_xIn_{1-x}N$ epilayers of appropriate compositions for HFETs on free-standing GaN (FS-GaN) substrates by MOVPE. We will purchase those wafers from Mitsubishi Chemical Corp. (MCC) or other suppliers. In case if necessary, we will dope carbon in the GaN base epitaxial layer to electrically isolate the semi-conducting FS-GaN. Most of equipments are already working. We will be grateful if AFRL could offer TEM observation opportunity.

2. Analyze those epilayers by a variety of optical and electrical measurements, such as static and time-resolved photoluminescence (PL and TRPL, respectively), spatially-resolved cathodoluminescence (CL), and Hall effect measurement. We will disclose how structural and point defects affect the internal quantum efficiency. We have a complete set of optical measurement system.

3. Fabricate *m*-plane AlGaN / GaN and AlInN / GaN heterostructures for HFET application. Because we have learnt that Kyma substrates are, unfortunately, not so good as a substrate for our purpose at the moment, we will either dope carbon in the underlayer GaN or use AlGaN layer underneath the channel. Because we do not have an accessible SdH facility, we would be grateful if AFRL could help us to measure the SdH oscillation and interface mobility.

4. Control the 2DEG density by doping the barriers with Si.

B Milestones and Deliverables Originally Planned

Following are the milestones:

Time	Goal/Milestone/Deliverable
4 months	Grow good structural and optical quality undoped *m*-plane $Al_xGa_{1-x}N$ and $Al_{1-x}In_xN$ films. Also obtain in-plane anisotropy of optical transitions.
7 months	Fabricate *m*-plane AlGaN/GaN and AlInN/GaN heterostructures.
9 months	Fabricate *m*-plane n-type AlGaN / GaN and AlGaN/GaN heterostructures by Si-doping.
10 months	Collaborate with AFRL to fabricate test FETs
End of project	Final report, Submit paper to E journal.

We will attend IWN2010 and ISCS to present what we will obtain through this project.

C Summary of the results (15 Apr. 2010 - 14 Aug. 2011 - approved Earthquake delay)

(0) Overview

We grew *m*-plane $Al_xGa_{1-x}N$ and $Al_{1-x}In_xN$ films and heterostructures on Mitsubishi Chemical Corp. (MCC) *m*-plane free-standing GaN (FS-GaN) substrates by MOVPE (and NH_3-MBE for some of AlGaN films). We began with characterizing state-of-the-art MCC FS-GaN substrate, in order to make clear the issues and advantages. As we knew the growth conditions of *m*-plane AlGaN, it did not take much time to just deposit AlGaN/GaN heterostructures, including Si-δ-doped barrier one. However, in case of NH_3-MBE, the growth of really flat *m*-plane AlGaN has been difficult due to the formation of striations along the *c*-axis. To assess the reason for this, we carried out spatially-resolved cathodoluminescence (SRCL) and time-resolved photoluminescence (TRPL) to find that the striations may originate from the formation of planar-defect network (PDN) located on prismatic (10-10) planes and pyramidal (1-10n) planes, which are often terminated by BSF. We spent most of time to obtain the films exhibiting monolayer atomic steps. We eventually succeeded in growing *m*-plane $Al_{0.25}Ga_{0.75}N$/GaN heterostructure. For *m*-plane $Al_{1-x}In_xN$, the surface of very thin, coherent films grown by MOVPE exhibited pretty smooth morphology. However, once the thickness exceeds the critical one, the morphology exhibited segmented rectangles, due presumably to tri-axial anisotropic lattice-mismatch. We finally asked AFRL to process the wafers. Unfortunately, because the substrate was semi-conducting, we were not able to electrically isolate them from the channel, so all the HFET structures exhibited leaky *I-V* characteristics and we did not see clear indication of 2DEG conduction at room temperature. Throughout this study, however, we obtained basic knowledge on the polarization characteristics of AlGaN and AlInN films suffering from anisotropic stresses.

(1) Polarization properties of *m*-plane $Al_xGa_{1-x}N$ films grown by MOVPE and NH_3-MBE on MCC *m*-plane free-standing GaN substrates

As a fundamental research for *m*-plane AlGaN, polarization ratios for the near-band-edge (NBE) optical transitions in *m*-plane $Al_xGa_{1-x}N$ epilayers suffering from anisotropic stresses were quantified. The light polarization direction altered from $E \perp c$ to $E // c$ at the AlN mole fraction, *x*, between 0.25 and 0.32, where *E* is the electric field component of the light and ⊥ and // represent perpendicular and parallel, respectively. To give a quantitative explanation for the result, energies and oscillator strengths of the exciton transitions involving three separate valence bands were calculated as functions of strains using the Bir-Pikus Hamiltonian. The calculation predicted that the lowest energy transition (E_1) is polarized to the *m*-axis normal to the surface (X_3) for $0<x\leq1$, meaning that E_1 emission is principally undetectable from the surface normal for any in-plane tensile strained $Al_xGa_{1-x}N$. The polarization direction of observable surface emission was predicted to alter from *c*-axis normal (X_1) to *c*-axis parallel (X_2) for the middle energy transition (E_2) and X_2 to X_1 for the highest energy transition (E_3) between x=0.25 and 0.32. The experimental results were consistently reproduced by the calculation.

(2) Impacts of anisotropic tilt mosaics of state-of-the-art *m*-plane freestanding GaN substrates on the structural and luminescent properties of *m*-plane $Al_xGa_{1-x}N$ epilayers

Impacts of grown-in anisotropic tilt mosaics of state-of-the-art *m*-plane FS-GaN substrates on the structural and luminescent properties of *m*-plane $Al_xGa_{1-x}N$ epilayers were investigated. The results of cross-sectional transmission-electron microscopy and transmission-electron diffraction analyses revealed the following planar-defects formation, even in mostly pseudomorphic

epilayers: (i) The formation of basal-plane stacking faults (BSFs) was hard to avoid in the case of lattice-mismatched $Al_xGa_{1-x}N$ thick film growth and (ii) the anisotropic greater *m*-plane tilt mosaic along the *a*-axis (twist in *c*-plane) of FS-GaN gave rise to pronounced formation of surface striations along the *c*-axis and planar-defect network (PDN) located on prismatic (10-10) planes and pyramidal (1-10*n*) planes, which are often terminated by BSF. These PDNs are assigned by SRCL and TRPL measurements to associate with a characteristic emission peak approximately 200–300 meV lower than the near-band-edge (NBE) emission peak. Based on our database made with the aid of the positron-annihilation technique, three deep-state CL bands are correlated with cation vacancies (V_{III}) and cation-vacancy complexes. The intensity of the emission band originating from V_{III}-oxygen complexes was weaker by more than two orders of magnitude than the NBE peak.

(3) MOVPE and characterization of *m*-plane $Al_{1-x}In_xN$ films on the freestanding GaN substrates

Epitaxial growth and characterizations were carried out on *m*-plane AlInN alloys. In order to eliminate the polarization discontinuity at the barrier/channel interface to obtain normally-off (*E*-mode) HFETs, the use of an AlInN barrier lattice-matched to GaN is one of the best solutions. As a preliminary result, we succeeded in growing epitaxial *m*-plane $Al_{1-x}In_xN$ alloys on the MCC *m*-plane FS-GaN substrates, and observed UV luminescence peaks ranging from 214 to 400 nm at room temperature.

(4) MOVPE and characterization of AlGaN / GaN and AlInN / GaN heterostructures

Heterostructures of AlGaN/GaN and AlInN/GaN were grown by MOVPE on the MCC *m*-plane FS-GaN substrates. As far as the barrier layers were thin enough, the surface exhibited smooth morphology with monolayer atomic step lines. We finally asked AFRL to process the wafers. However, because the substrate was semi-conducting, we were not able to electrically isolate them from the channel, so all the HFET structures exhibited leaky *I-V* characteristics and we did not see clear indication of 2DEG conduction at room temperature.

D Technical Reports

(1) Polarization properties of *m*-plane $Al_xGa_{1-x}N$ films grown by MOVPE and NH_3-MBE on MCC *m*-plane free-standing GaN substrates
-- Optics Express 19, A1008 (2011) attached in the next 14 pages --

Optical polarization properties of *m*-plane $Al_xGa_{1-x}N$ epitaxial films grown on *m*-plane freestanding GaN substrates toward nonpolar ultraviolet LEDs

Kouji Hazu[*] and Shigefusa F. Chichibu

Center for Advanced Nitride Technology, Institute of Multidisciplinary Research for Advanced Materials, Tohoku University, 2-1-1 Katahira, Aoba, Sendai 980-8577, Japan
[*]*chichibulab@yahoo.co.jp*

Abstract: Light polarization characteristics of the near-band-edge optical transitions in *m*-plane $Al_xGa_{1-x}N$ epilayers suffering from anisotropic stresses are quantitatively explained. The epilayers were grown on an *m*-plane freestanding GaN substrate by both ammonia-source molecular beam epitaxy and metalorganic vapor phase epitaxy methods. The light polarization direction altered from $E \perp c$ to $E // c$ at the AlN mole fraction, x, between 0.25 and 0.32, where E is the electric field component of the light and $\perp$ and // represent perpendicular and parallel, respectively. To give a quantitative explanation for the result, energies and oscillator strengths of the exciton transitions involving three separate valence bands are calculated as functions of strains using the Bir-Pikus Hamiltonian. The calculation predicts that the lowest energy transition (E_1) is polarized to the *m*-axis normal to the surface (X_3) for $0<x\leq1$, meaning that E_1 emission is principally undetectable from the surface normal for any in-plane tensile strained $Al_xGa_{1-x}N$. The polarization direction of observable surface emission is predicted to alter from *c*-axis normal (X_1) to *c*-axis parallel (X_2) for the middle energy transition (E_2) and X_2 to X_1 for the highest energy transition (E_3) between x = 0.25 and 0.32. The experimental results are consistently reproduced by the calculation.

OCIS codes: (160.6000) Semiconductor materials; (300.6250) Spectroscopy, condensed matter.

References and links

1. Y. Taniyasu, M. Kasu, and T. Makimoto, "An aluminium nitride light-emitting diode with a wavelength of 210 nanometres," Nature **441**(7091), 325–328 (2006).
2. Y. Narukawa, M. Ichikawa, D. Sanga, M. Sano, and T. Mukai, "White light emitting diodes with super-high luminous efficacy," J. Phys. D Appl. Phys. **43**(35), 354002 (2010).
3. H. Tsuzuki, F. Mori, K. Takeda, M. Iwaya, S. Kamiyama, H. Amano, I. Akasaki, H. Yoshida, M. Kuwabara, Y. Yamashita, and H. Kan, "Novel UV devices on high-quality AlGaN using grooved underlying layer," J. Cryst. Growth **311**(10), 2860–2863 (2009).
4. X. Hu, J. Deng, J. P. Zhang, A. Lunev, Y. Bilenko, T. Katona, M. S. Shur, R. Gaska, M. Shatalov, and A. Khan, "Deep ultraviolet light-emitting diodes," Phys. Stat. Solidi A **203**(7), 1815–1818 (2006).
5. H. Hirayama, N. Noguchi, and N. Kamata, "222 nm Deep-Ultraviolet AlGaN Quantum Well Light-Emitting Diode with Vertical Emission Properties," Appl. Phys. Express **3**(3), 032102 (2010).
6. D. A. Miller, D. S. Chemla, T. C. Damen, A. C. Gossard, W. Wiegmann, T. H. Wood, and C. A. Burrus, "Band-Edge Electroabsorption in Quantum Well Structures: The Quantum-Confined Stark Effect," Phys. Rev. Lett. **53**(22), 2173–2176 (1984).
7. P. Waltereit, O. Brandt, A. Trampert, H. T. Grahn, J. Menniger, M. Ramsteiner, M. Reiche, and K. H. Ploog, "Nitride semiconductors free of electrostatic fields for efficient white light-emitting diodes," Nature **406**(6798), 865–868 (2000).
8. M. D. Craven, P. Waltereit, J. S. Speck, and S. P. DenBaars, "Well-width dependence of photoluminescence emission from *a*-plane GaN/AlGaN multiple quantum wells," Appl. Phys. Lett. **84**(4), 496–498 (2004).

#149903 - $15.00 USD Received 24 Jun 2011; revised 29 Jun 2011; accepted 30 Jun 2011; published 1 Jul 2011

9. T. Koida, S. F. Chichibu, T. Sota, M. D. Craven, D. A. Haskell, J. S. Speck, S. P. DenBaars, and S. Nakamura, "Improved quantum efficiency in nonpolar (110) AlGaN/GaN quantum wells grown on GaN prepared by lateral epitaxial overgrowth," Appl. Phys. Lett. **84**(19), 3768–3770 (2004).
10. J. S. Speck and S. F. Chichibu, "Nonpolar and Semipolar Group III Nitride-Based Materials," MRS Bull. **34**(05), 304–312 (2009).
11. H. Masui, T. J. Baker, M. Iza, H. Zhong, S. Nakamura, and S. P. DenBaars, "Light-polarization characteristics of electroluminescence from InGaN/GaN light-emitting diodes prepared on (112)-plane GaN," J. Appl. Phys. **100**(11), 113109 (2006).
12. M. Masui, T. J. Baker, R. Sharma, P. M. Pattison, M. Iza, H. Zhong, S. Nakamura, and S. P. DenBaars, "First-Moment Analysis of Polarized Light Emission from InGaN/GaN Light-Emitting Diodes Prepared on Semipolar Planes," Jpn. J. Appl. Phys. **45**(34), L904–L906 (2006).
13. R. Sharma, P. M. Pattison, H. Masui, R. M. Farrell, T. J. Baker, B. A. Haskell, F. Wu, S. P. DenBaars, J. S. Speck, and S. Nakamura, "Demonstration of a semipolar (10) InGaN/GaN green light emitting diode," Appl. Phys. Lett. **87**(23), 231110 (2005).
14. K. Okamoto, H. Ohta, D. Nakagawa, M. Sonobe, J. Ichihara, and H. Takasu, "Dislocation-Free *m*-Plane InGaN/GaN Light-Emitting Diodes on *m*-Plane GaN Single Crystals," Jpn. J. Appl. Phys. **45**(45), L1197–L1199 (2006).
15. M. C. Schmidt, K.-C. Kim, H. Sato, N. Fellows, H. Masui, S. Nakamura, S. P. DenBaars, and J. S. Speck, "High Power and High External Efficiency *m*-Plane InGaN Light Emitting Diodes," Jpn. J. Appl. Phys. **46**(7), L126–L128 (2007).
16. K. Fujito, K. Kiyomi, T. Mochizuki, H. Oota, H. Namita, S. Nagao, and I. Fujimura, "High-quality nonpolar *m*-plane GaN substrates grown by HVPE," Phys. Stat. Solidi A **205**(5), 1056–1059 (2008).
17. K. Iso, H. Yamada, H. Hirasawa, N. Fellows, M. Saito, K. Fujito, S. P. DenBaars, J. S. Speck, and S. Nakamura, "High Brightness InGaN/GaN Light Emitting Diode on Nonpolar *m*-plane Bulk GaN Substrate," Jpn. J. Appl. Phys. **46**(40), L960–L962 (2007).
18. S. F. Chichibu, A. Uedono, T. Onuma, S. P. DenBaars, U. K. Mishra, J. S. Speck, and S. Nakamura, "Impact of Point Defects on the Luminescence Properties of (Al,Ga)N," Mater. Sci. Forum **590**, 233–248 (2008).
19. T. Onuma, K. Hazu, A. Uedono, T. Sota, and S. F. Chichibu, "Identification of extremely radiative nature of AlN by time-resolved photoluminescence," Appl. Phys. Lett. **96**(6), 061906 (2010).
20. S. F. Chichibu, T. Onuma, K. Hazu, and A. Uedono, "Major impacts of point defects and impurities on the carrier recombination dynamics in AlN," Appl. Phys. Lett. **97**(20), 201904 (2010).
21. K. Domen, K. Kondo, A. Kuramata, and T. Tanahasi, "Gain analysis for surface emission by optical pumping of wurtzite GaN," Appl. Phys. Lett. **69**(1), 94–96 (1996).
22. T. Ohtoshi, A. Niwa, and T. Kuroda, "Dependence of optical gain on crystal orientation in wurtzite-GaN strained quantum-well lasers," J. Appl. Phys. **82**(4), 1518–1520 (1997).
23. B. Gil and A. Alemu, "Optical anisotropy of excitons in strained GaN epilayers grown along the <100> direction," Phys. Rev. B **56**(19), 12446–12453 (1997).
24. A. Alemu, B. Gil, M. Julier, and S. Nakamura, "Optical properties of wurtzite GaN epilayers grown on *A*-plane sapphire," Phys. Rev. B **57**(7), 3761–3764 (1998).
25. S.-H. Park and S.-L. Chuang, "Crystal-orientation effects on the piezoelectric field and electronic properties of strained wurtzite semiconductors," Phys. Rev. B **59**(7), 4725–4737 (1999).
26. S. Ghosh, P. Waltereit, O. Brandt, H. T. Grahn, and K. H. Ploog, "Electronic band structure of wurtzite GaN under biaxial strain in the *M* plane investigated with photoreflectance spectroscopy," Phys. Rev. B **65**(7), 075202 (2002).
27. L. R. Ram-Mohan, A. M. Girgis, J. D. Albrecht, and C. W. Litton, "Wavefunction engineering of layered wurtzite semiconductors grown along arbitrary crystallographic directions," Superlattices Microstruct. **39**(6), 455–477 (2006).
28. S. –H. Park and D. Ahn, "Depolarization effects in (112)-oriented InGaN/GaN quantum well structures," Appl. Phys. Lett. **90**, 013505 1–3 (2007).
29. A. A. Yamaguchi, "Anisotropic Optical Matrix Elements in Strained GaN Quantum Wells on Semipolar and Nonpolar Substrates," Jpn. J. Appl. Phys. **46**(33), L789–L791 (2007).
30. A. A. Yamaguchi, "Anisotropic optical matrix elements in strained GaN-quantum wells with various substrate orientations," Phys. Stat. Solidi C **5**(6), 2329–2332 (2008).
31. J. Bhattacharyya, S. Ghosh, and H. T. Grahn, "Optical polarization properties of interband transitions in strained group-III-nitride alloy films on GaN substrates with nonpolar orientation," Appl. Phys. Lett. **93**(5), 051913 (2008).
32. G. L. Bir and G. E. Pikus, *Symmetry and Strain-Induced Effect in Semiconductors*, (Wiley, New York, 1974).
33. T. Hoshi, K. Hazu, K. Ohshita, M. Kagaya, T. Onuma, K. Fujito, H. Namita, and S. F. Chichibu, "Impacts of anisotropic lattice relaxation on crystal mosaicity and luminescence spectra of m-plane $Al_xGa_{1-x}N$ films grown on m-plane freestanding GaN substrates by NH_3 source molecular beam epitaxy," Appl. Phys. Lett. **94**(7), 071910 (2009).
34. S. F. Chichibu, H. Yamaguchi, L. Zhao, M. Kubota, K. Okamoto, and H. Ohta, "Optical properties of nearly stacking-fault-free *m*-plane GaN homoepitaxial films grown by metal organic vapor phase epitaxy on low defect density freestanding GaN substrates," Appl. Phys. Lett. **93**(12), 129901 (2008) (erratum).
35. R. People and J. C. Bean, "Calculation of critical layer thickness versus lattice mismatch for Ge_xSi_{1-x}/Si strained-layer heterostructures," Appl. Phys. Lett. **47**(3), 322–324 (1985).
36. T. Onuma, T. Koyama, A. Chakraborty, M. McLaurin, B. A. Haskell, P. T. Fini, S. Keller, S. P. DenBaars, J. S. Speck, S. Nakamura, U. K. Mishra, T. Sota, and S. F. Chichibu, "Radiative and nonradiative lifetimes in

#149903 - $15.00 USD Received 24 Jun 2011; revised 29 Jun 2011; accepted 30 Jun 2011; published 1 Jul 2011

nonpolar *m*-plane $In_xGa_{1-x}N$/GaN multiple quantum wells grown on GaN templates prepared by lateral epitaxial overgrowth," J. Vac. Sci. Technol. B **25**(4), 1524–1528 (2007).
37. E. C. Young, C. S. Gallinat, F. Wu, and J. S. Speck, "Ammonia molecular beam epitaxy of *m*-plane GaN and InGaN for long wavelength optoelectronics," presented at International Workshop on Nitride Semiconductors (IWN), Montreux, Switzerland, 6–10, Oct. 2008.
38. S. F. Chichibu, H. Yamaguchi, L. Zhao, M. Kubota, T. Onuma, and H. Ohta, "Improved characteristics and issues of m-plane freestanding GaN substrates by metalorganic vapor phase epitaxy," Appl. Phys. Lett. **93**(15), 151908 (2008).
39. A. Shikanai, T. Azuhata, T. Sota, S. Chichibu, A. Kuramata, K. Horino, and S. Nakamura, "Biaxial strain dependence of exciton resonance energies in wurtzite GaN," J. Appl. Phys. **81**(1), 417–424 (1997).
40. T. Onuma, T. Shibata, K. Kosaka, K. Asai, S. Sumiya, M. Tanaka, T. Sota, A. Uedono, and S. F. Chichibu, "Free and bound exciton fine structures in AlN epilayers grown by low-pressure metalorganic vapor phase epitaxy," J. Appl. Phys. **105**(2), 023529 (2009).
41. T. Onuma, S. F. Chichibu, A. Uedono, T. Sota, P. Cantu, T. M. Katona, J. F. Keading, S. Keller, U. K. Mishra, S. Nakamura, and S. P. DenBaars, "Radiative and nonradiative processes in strain-free $Al_xGa_{1-x}N$ films studied by time-resolved photoluminescence and positron annihilation techniques," J. Appl. Phys. **95**(5), 2495–2504 (2004).
42. B. Monemar, "Fundamental energy gap of GaN from photoluminescence excitation spectra," Phys. Rev. B **10**(2), 676–681 (1974).
43. H. Ikeda, T. Okamura, K. Matsukawa, T. Sota, M. Sugawara, T. Hoshi, P. Cantu, R. Sharma, J. F. Kaeding, S. Keller, U. K. Mishra, K. Kosaka, K. Asai, S. Sumiya, T. Shibata, M. Tanaka, J. S. Speck, S. P. DenBaars, S. Nakamura, T. Onuma, and S. F. Chichibu, ""Impact of strain on free-exciton resonance energies in wurtzite AlN," J. Appl. Phys. **103**(8), 089901 (2008) (erratum).
44. H. G. Grimmeiss and B. Monemar, "Low-Temperature Luminescence of GaN," J. Appl. Phys. **41**(10), 4054–4058 (1970).

1. Introduction

Wurtzite $Al_xGa_{1-x}N$ alloys are an attractive candidate for realizing ultraviolet (UV) light emitters and high-power high-frequency electronic devices, because they have large bandgap energies ranging from 3.43 eV (x = 0) to 6.01 eV (x = 1) and they principally are a hard material. Recently, a 210-nm electroluminescence (EL) has been demonstrated for *c*-plane AlN *p*-*i*-*n* homojunction light-emitting-diodes (LEDs) [1]. However, the external quantum efficiency (EQE) was as low as 10^{-6}% at 300 K, which was extremely lower than that of conventional blue or violet InGaN LEDs being ~84.3% for a 444 nm InGaN LED [2]. To improve overall performance of AlGaN-based deep UV (DUV) LEDs, many researchers have been trying to improve AlGaN quality and to optimize the multiple-quantum-well (MQW) design. As a consequence, the EQE values of 6.7% for a 345 nm LED [3], over 3% for 244-280 nm LEDs [4], and 0.003% for a 222 nm LED [5] have been achieved. Obviously, the values are still insufficient for practical use.

Currently, above mentioned UV LEDs are grown along the *c*-axis. In these structures, spontaneous and piezoelectric polarization discontinuity at the heterointerfaces induces the electric fields in the structure, which are parallel to the growth direction. These electric fields separate the electron (*e*) and hole (*h*) wavefunctions to the opposite interfaces of quantum wells (QWs), resulting in low optical efficiency and the forward-current-induced blueshift of the *c*-plane LEDs. These effects are called as quantum-confined Stark effects (QCSEs) [6]. To avoid QCSEs in (Al, In, Ga)N heterostructures, epitaxial growths on off-polar orientations such as (110) *a*-plane, and (100) *m*-plane (nonpolar planes) and (112), (201), and (10) planes (semipolar planes) have been attracting attentions [7–13]. In 2006, *m*-plane InGaN LEDs, whose EQEs were 3.1% at 435 nm [14] and 38.9% at 405 nm [15], have been demonstrated using the low threading-dislocation (TD) density, free-standing (FS) GaN substrates [16], which were sliced from a sub-cm-thick *c*-plane FS-GaN grown by halide vapor phase epitaxy (HVPE). Schematic drawing of a *c*-plane FS-GaN boule grown on a *c*-plane Al_2O_3 substrate and a sliced *m*-plane FS-GaN is shown in Fig. 1(a). Subsequently, longer wavelength, 468 nm *m*-plane InGaN LEDs with EQEs higher than 15% have been reported [17]. However, drastic decrease in the output power cannot be suppressed for the *m*-plane InGaN LEDs whose peak wavelength is longer than 470 nm. The reason for this is often attributed to the degradation of crystal quality, which is caused by the low growth temperatures required for achieving high InN mole fraction InGaN. To the best of our knowledge, nonpolar DUV LEDs have not been reported yet.

#149903 - $15.00 USD Received 24 Jun 2011; revised 29 Jun 2011; accepted 30 Jun 2011; published 1 Jul 2011

Possible reason for the low EQEs of DUV LEDs is the increase of TD and point defect densities [18] with increasing AlN mole fraction *x*. Indeed, high quality GaN and AlGaN alloys of reduced nonaradiative recombination center (NRC) concentration are indispensable to realize high efficiency UV LEDs. In addition to the extended defects such as TDs and stacking faults (SFs), there exist microscopic ones such as point defects, complexes, and impurities (O, C, and Si) in (Al, In, Ga)N crystals. From the results of the time-resolved photoluminescence (TRPL) and positron annihilation measurements, the origin of NRCs have been proposed to be certain point-defect complexes containing cation vacancies (V_{III}-X) [18]. Quite recently, radiative lifetime (τ_R) of AlN has been shown to increase with increasing point defect and impurity concentrations [19,20], meaning that point defects play an important role in determining the recombination dynamics.

In order to optimize nonpolar $Al_xGa_{1-x}N$ LED structures, the oscillator strengths (f) of three interband optical transitions in ideal, defect-free ones must be quantified as functions of light polarization direction and strains. With respect to the effect of anisotropic strain, optical polarization properties of (Al, In, Ga)N films and QWs of various orientations have been investigated [21–31]. Among them, Bhattacharyya *et al*. [31] have calculated the light polarization characteristics of the transitions involving three separate valence bands for *m*-plane $Al_xGa_{1-x}N$ films on GaN, which suffer from anisotropic tensile stresses. They have estimated the anticrossing AlN mole fraction $x = 0.10$, and predicted that the lowest energy transition of $Al_xGa_{1-x}N$ is predominantly polarization parallel to the substrate normal.

In this paper, the results of polarized CL measurement on *m*-plane $Al_xGa_{1-x}N$ epilayers grown on the *m*-plane FS-GaN substrate are shown. All of the epilayers grown by ammonia-source molecular beam epitaxy (NH_3-MBE) and metalorganic vapor phase epitaxy (MOVPE) suffer from in-plane anisotropic tensile stresses. The results are quantitatively explained by calculating the transition energies and oscillator strengths of excitonic transitions involving three separate valence bands, as functions of in-plane strains. For the calculation, Bir-Pikus Hamiltonian [32] was used without fitting parameters.

2.Experimental details and results

Samples investigated are approximately 100 to 400-nm-thick *m*-plane $Al_xGa_{1-x}N$ epilayers grown on an 1-μm-thick GaN homoepitaxial layer, which was grown on the *m*-plane FS-GaN substrates [16]. The surface of as-received substrates was inspected by atomic-force microscopy (AFM) and found to have smooth morphology with monolayer atomic steps [16,33,34]. However, the x-ray rocking curves (XRCs) exhibited multiple-peak or asymmetric line shapes [33], as shown in Fig. 1(b). This multiple grain structure principally originates from the bowing of the original *c*-plane FS-GaN. Because the state-of-the-art *m*-plane FS-GaN [16] is prepared by slicing nearly 1-cm-thick *c*-plane FS-GaN grown in Ga-polar [0001] direction, the *c*-plane tilt (including the wafer bowing) and twist mosaics of the initial crystal are transferred to blurring of the *c*-axis and the greater *m*-plane tilt mosaic along the *a*-axis, respectively, as shown schematically in Fig. 1(a). For instance, the values of full width at half-maximum (FWHM) of XRCs for the present substrate were $\Delta\omega_{mc} = 76$ and $\Delta\omega_{ma} = 110$ arcsec for the (100) diffraction along <0001> and <110> azimuths, respectively, [Fig. 1(b)] and $\Delta\omega_r = 100$ arcsec for the (102) diffraction. The TD and stacking fault (SF) densities were lower than 5×10^6 cm^{-2} and 1×10^3 cm^{-1}, respectively [33,34]. The NH_3-MBE of *m*-plane $Al_xGa_{1-x}N$ epilayers ($0 \le x \le 0.70$) were carried out at 870-970 °C using metallic Ga (7N) and Al (6N) sources. The beam-equivalent-pressures of metallic Ga and NH_3 were (2.1-4.0) $\times 10^{-5}$ and (1.3-4.1) $\times 10^{-2}$ Pa, respectively. The growth details are found in Ref. 35. A 150-nm-thick $Al_{0.73}Ga_{0.27}N$ and approximately 2.1-μm-thick AlN epilayers were grown at 1120 °C on the same *m*-plane FS-GaN substrates by MOVPE. The reactor pressure was 2.02×10^4 Pa. Trimethylaluminum, triethylgallium, and NH_3 were used as the precursors.

#149903 - $15.00 USD Received 24 Jun 2011; revised 29 Jun 2011; accepted 30 Jun 2011; published 1 Jul 2011

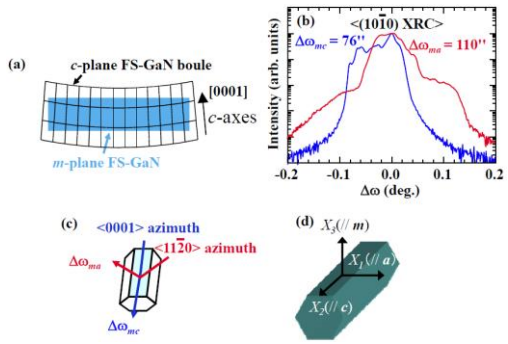

Fig. 1. (a) Schematic drawing of a *c*-plane FS-GaN boule grown on a *c*-plane Al_2O_3 substrate by HVPE and a sliced *m*-plane FS-GaN. (b) X-ray rocking curves for the (100) diffraction of the *m*-plane FS-GaN. The x-rays were irradiated along the *c*-axis or *a*-axis, as shown in panel (c). (d) Schematic diagram of the notations of three axes.

High-resolution x-ray diffraction (XRD) measurements were carried out using a four-crystal monochromator and an analyzer crystal (Bruker D8). A system with a one-dimensional detector array was used to obtain the x-ray reciprocal space mapping (X-RSM) images. The *m*-plane $Al_xGa_{1-x}N$ epilayers of low x ($0<x\leq0.32$) were confirmed by X-RSM to grow coherently on the GaN base layers. Other high AlN mole fraction epilayers ($x\geq0.35$) were partially or nearly fully relaxed. Due to the tensile strain, the epilayers of $x\geq0.35$ had macroscopic surface cracks. Representative X-RSM images for the pseudomorphic $Al_{0.25}Ga_{0.75}N$ and mostly relaxed $Al_{0.70}Ga_{0.30}N$ epilayers grown by NH_3-MBE are displayed in Fig. 2. In each panel, the ideal location for strain-free AlN is shown by a closed (red) circle. We note that critical layer thicknesses calculated by the model given by People and Bean [35] are 202 nm for x = 0.25 and 31 nm for x = 0.52, taking in-plane anisotropic lattice and thermal-expansion mismatches into account. Because both the pseudomorphic and relaxed films suffered from anisotropic strains, x values were calculated from the out-of-plane (*m*-axis) and in-plane (*c*- and *a*-axes) lattice parameters, which were obtained from a 2θ-ω scan for the (100) XRD and X-RSM results for (201) and (120) diffractions, respectively (see Fig. 2, for example). The relation $\varepsilon_{X_3X_3}=\left(-C_{12}\varepsilon_{X\,X_1}-C_{13}\varepsilon_{X_2X_2}\right)/C_{11}$ was used, where $\varepsilon_{X_3X_3}$, $\varepsilon_{X_1X_1}$ and $\varepsilon_{X_2X_2}$ are the strains along *m*-, *a*-, and *c*-axes and C_{ij} are the elastic stiffness constants of $Al_xGa_{1-x}N$ alloys were assumed to obey [36] Vegard's law. In-plane tensile strains increased with x for the pseudomorphic (coherently grown) films, as shown in Fig. 3(a). Conversely, the strains were gradually relaxed by the partial relaxation for x>0.32. For the quantitative discussion of polarization properties, we define the notations for the three axes: X_1 (perpendicular to the *c*-axis in the growth plane); X_2 (parallel to the *c*-axis in the growth plane); and X_3 (normal to the growth plane), as shown in Fig. 1(d).

#149903 - $15.00 USD Received 24 Jun 2011; revised 29 Jun 2011; accepted 30 Jun 2011; published 1 Jul 2011

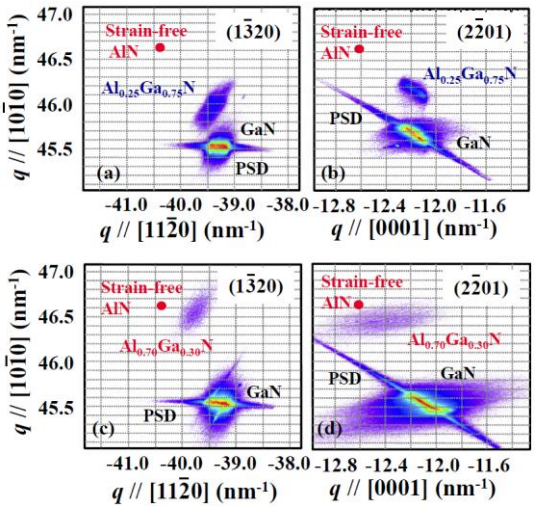

Fig. 2. Representative X-RSM images for the pseudomorhic *m*-plane $Al_{0.25}Ga_{0.75}N$ epilayer grown on the *m*-plane FS-GaN taken in the vicinity of (a) (130) and (b) (201) diffraction spots. The X-RSM images for partially lattice-relaxed $Al_{0.70}Ga_{0.30}N$ epilayers taken for (c) (120) and (d) (201) diffractions. Both the epilayers were grown by NH_3-MBE. The closed circle in each panel shows the location of strain-free AlN, for comparison.

The surface of the MOVPE epilayers exhibits well-aligned 0.26-nm-high monolayer atomic step lines. In contrast, the MBE epilayers exhibit surface striations parallel to the *c*-axis. We note that the striations have already been formed during the underlayer GaN growth [33]. Therefore, different from the MOVPE case, it seems difficult for NH_3-MBE [33,37] to eliminate such striations, even for the binary GaN growth. The reason for this may be an inappropriate surface preparation or insufficient migration of Ga adatoms due to lower growth temperature (T_g) in comparison with MOVPE, because NH_3-MBE is a surface-sensitive growth method. Indeed, the depth of the striations in the $Al_xGa_{1-x}N$ films was deeper than the GaN case, where Al-containing materials need higher T_g to ensure sufficient surface migration. Here, we note that the in-plane polar direction of the epilayers was confirmed by convergent-beam electron diffraction (CBED) measurement to be the same as the substrate.

Despite the presence of such surface striations, all the *m*-plane $Al_xGa_{1-x}N$ films grown by NH_3-MBE exhibit a single (100) XRD peak, similar to the case for the MOVPE films. The results mean that both the MOVPE and MBE epilayers did not show noticeable phase separation or compositional ordering along the *m*-axis. However, similar to FS-GaN, XRCs for the pseudomorphic $Al_xGa_{1-x}N$ films exhibit a multiple-peak or asymmetric line shape. Because this is also the case for both underlying GaN homoepitaxial films [34,38] and the substrate [16], the multidomain structure (bowing) of the original *c*-plane FS-GaN must be the major reason [see Fig. 1(a)]. In contrast, relaxed $Al_xGa_{1-x}N$ films exhibit broad but single-peaked XRCs. In those films, the multiple domain fine structure seems to be hidden due to the broadness of the line shape.

As long as coherent growth was maintained, $\Delta\omega_{mc}$ of the $Al_xGa_{1-x}N$ epilayers are the same as the substrate, regardless of the presence of striations, as shown in Fig. 3(b). The result is similar to the case with pseudomorphic *m*-pane $In_xGa_{1-x}N$ ($x \leq 0.14$) epilayers [38] grown on the *m*-plane FS-GaN prepared by the same provider (Mitsubishi Chemical Holdings Group). However, $\Delta\omega_{ma}$ and $\Delta\omega_r$ immediately increased for $0<x\leq0.25$, presumably because the twist mosaic along the *c*-axis of the initial *c*-plane FS-GaN was exaggerated by the lattice and thermal-expansion mismatches between AlGaN and GaN during surface-sensitive NH_3-MBE. This must be another origin for the deeper striations in the $Al_xGa_{1-x}N$ films, in comparison with GaN films. The broader horizontal width of the (120) X-RSM spot the $Al_{0.25}Ga_{0.75}N$ epilayer [Fig. 2(a)] also reflects the result. For the $Al_{0.32}Ga_{0.68}N$ film, $\Delta\omega$ values were larger than those for $x\leq0.25$, reflecting the increase in misfit dislocation densities.

#149903 - $15.00 USD Received 24 Jun 2011; revised 29 Jun 2011; accepted 30 Jun 2011; published 1 Jul 2011

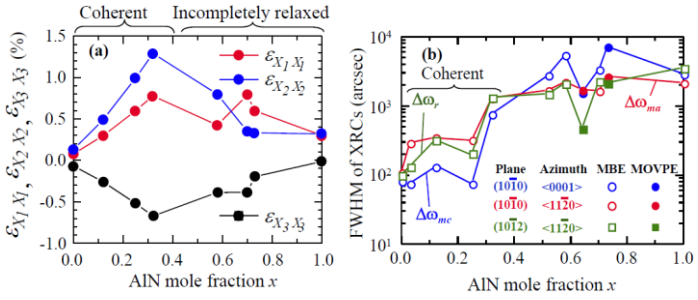

Fig. 3. (a) FWHM values for the XRCs ($\Delta\omega_{mc}$, $\Delta\omega_{ma}$, and $\Delta\omega_r$) of *m*-plane $Al_xGa_{1-x}N$ epilayers grown by NH_3-MBE and MOVPE. (b) Strain components $\varepsilon_{X_1X_1}$, $\varepsilon_{X_2X_2}$, and $\varepsilon_{X_3X_3}$ of the *m*-plane $Al_xGa_{1-x}N$ films as a function of AlN mole fraction *x*.

Steady-state CL was excited with an electron beam operated at 3.0 kV. The probe current density was 1.0×10^{-2} A/cm^2 at sample. The emission was dispersed by a 30-cm-focal-length grating monochromator, and detected using a multi-channel charge-coupled device. A Glan-Thompson prism polarizer was used for the polarized CL measurement. Polarized near-band-edge (NBE) CL spectra at 12 K of the *m*-plane $Al_xGa_{1-x}N$ films are shown as a function of *x* in Fig. 4(a). The intensities are normalized to that of stronger polarization direction (X_1 or X_2) for each *x*. The entire spectra shifted to the higher energy with increasing *x*, although some of them exhibited double emission peaks. As shown, the light polarization direction altered from X_1 to X_2 between x = 0.25 and 0.32. The value of polarization ratio ρ was defined as $(I_{X_1} - I_{X_2})/(I_{X_1} + I_{X_2})$, where I_{X_2} and I_{X_1} are the spectrally-integrated CL intensities of the NBE emission. The values are plotted by closed circles in Fig. 4(b).

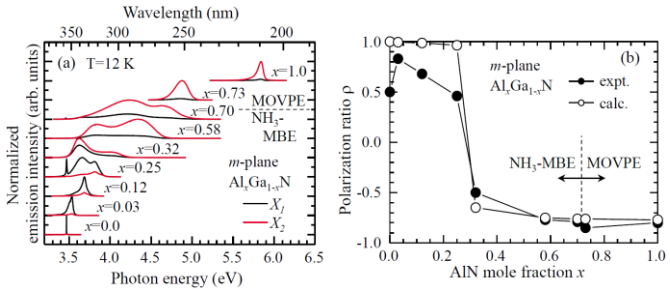

Fig. 4. (a) Polarized CL spectra at 12 K of *m*-plane $Al_xGa_{1-x}N$ epilayers grown on the *m*-plane FS-GaN substrates. (b) Polarization ratios, which are defined as $(I_{X_1} - I_{X_2})/(I_{X_1} + I_{X_2})$, of the $Al_xGa_{1-x}N$ films as a function of AlN mole fraction *x*. Corresponding values calculated using the relative oscillator strengths are also shown. The films of $x \leq 0.70$ were grown by NH_3-MBE and $x \geq 0.73$ were grown by MOVPE.

3. Theoretical analysis

To quantitatively explain the experimental findings, the energies and oscillator strengths of the interband transitions involving three separate valence bands (VBs) are calculated using the Bir-Pikus Hamiltonian [32], taking the anisotropic strains into account. At the Γ point, the states at the conduction band minimum (CBM) have an atomic *s* orbital with wavefunctions of $|S\rangle$ symmetry. The three valence band maximum (VBM) states have atomic *p* orbitals with wavefunctions of a combination of $|X\rangle$, $|Y\rangle$, and $|Z\rangle$ symmetries. For simplicity, excitonic effects are neglected in the calculation. The Hamiltonian for the strain dependence of VB is given by the following 6 × 6 matrix

#149903 - $15.00 USD Received 24 Jun 2011; revised 29 Jun 2011; accepted 30 Jun 2011; published 1 Jul 2011

$$H = \begin{bmatrix} F & 0 & -H^* & 0 & K^* & 0 \\ 0 & G & \Delta & -H^* & 0 & K^* \\ -H & \Delta & \lambda & 0 & I^* & 0 \\ 0 & -H & 0 & \lambda & \Delta & I^* \\ K & 0 & I & \Delta & G & 0 \\ 0 & K & 0 & I & 0 & F \end{bmatrix},$$

where

$$F = \Delta_1 + \Delta_2 + \lambda + \theta,$$

$$G = \Delta_1 - \Delta_2 + \lambda + \theta,$$

$$H = i\left(A_6 k_z k_+ + A_7 k_+ + D_6 \varepsilon_{z+}\right),$$

$$I = i\left(A_6 k_z k_+ - A_7 k_+ + D_6 \varepsilon_{z+}\right),$$

$$K = A_5 k_+^2 + D_5 \varepsilon_+,$$

$$\lambda = A_1 k_z^2 + A_2 k_\perp^2 + D_1 \varepsilon_{zz} + D_2\left(\varepsilon_{xx} + \varepsilon_{yy}\right),$$

$$\theta = A_3 k_z^2 + A_4 k_\perp^2 + D_3 \varepsilon_{zz} + D_4\left(\varepsilon_{xx} + \varepsilon_{yy}\right),$$

$$\Delta = \sqrt{2}\Delta_3,$$

$$k_\perp^2 = k_x^2 + k_y^2,$$

$$k_+ = k_x + ik_y,$$

$$\varepsilon_{z+} = \varepsilon_{xz} + i\varepsilon_{yz},$$

and

$$\varepsilon_+ = \varepsilon_{xx} - \varepsilon_{yy} + 2i\varepsilon_{xy}. \quad (1)$$

The parameters D_j (j = 1 to 6) denote the deformation potential constants for the valence band and A_j (j = 1 to 7) are Luttinger parameters, and ε_{lm} and k_l (l, m = X_1, X_2, X_3) are the strain and wavevector components, respectively. Here we assume that non-diagonal elements of the strain tensor are zero. $\Delta_1 = \Delta_{cr}$ is the crystal field splitting, while $3\Delta_2 = 3\Delta_3 = \Delta_{so}$ are the spin-orbit splitting under quasi-cubic approximation. The basis functions of Bir-Pikus Hamiltonian are $\left(1/\sqrt{2}\right)\left|X+iY,\alpha\right\rangle$, $\left(1/\sqrt{2}\right)\left|X+iY,\beta\right\rangle$, $\left(1+\sqrt{2}\right)\left|X-iY,\alpha\right\rangle$, $\left(1/\sqrt{2}\right)\left|X-iY,\beta\right\rangle$, , $\left|Z,\alpha\right\rangle$ and $\left|Z,\beta\right\rangle$. Here |α⟩ and |β⟩ denote the spin-wave functions corresponding to up spin and down spin, respectively. The method described here is universal, and Bhattacharyya *et al*. [31] have also used the same approach for calculating the electronic states of *m*-plane (Al, In, Ga)N alloys.

The exciton transition energies are obtained from the band energies and exciton binding energy:

$$E_j = E^* + E^c - E_j^v - E_{ex}^b,$$

#149903 - $15.00 USD Received 24 Jun 2011; revised 29 Jun 2011; accepted 30 Jun 2011; published 1 Jul 2011

where $E^* = E_g + \Delta_1 + \Delta_2$. The parameters E_g, E^c, E^v_j, and E^b_{ex} are the band gap energy, the CBM energy, the VBM energies, and the exciton binding energy, respectively. The E^b_{ex} values for the *A*-, *B*-, and *C*-transition were set identical to 26 meV [39] for GaN and 51.3 meV for AlN [40].

The oscillator strength components for the transitions are obtained from momentum matrix elements $\left|\left\langle \Psi^{CB}\left|p_l\right|\Psi^{VB}\right\rangle\right|^2$ with l = x, y, and z. Here, $\left\langle \Psi^{CB}\right| = \left\langle S\right|$ and $\left|\left\langle \Psi^{VB}\right|\right\rangle = a_1\left|X\right\rangle + a_2\left|Y\right\rangle + a_3\left|Z\right\rangle$ represent the orbital parts of the CB and VB basis functions, respectively. The coefficients a_j are obtained by determining the eigenvectors of Hamiltonian. The *relative* values of $\left|\left\langle S\left|p_x\right|X\right\rangle\right|^2$, $\left|\left\langle S\left|p_y\right|Y\right\rangle\right|^2$, and $\left|\left\langle S\left|p_Z\right|X\right\rangle\right|^2$ are set unity under the quasi-cubic approximation, $\sum_{i=1}^{3} f_{i,\beta} = 1$. The calculations stated herein are carried out exclusively at **k** = 0, meaning that the 6 × 6 matrix was effectively treated as 3 × 3.

For the practical calculation on $Al_xGa_{1-x}N$ alloy films, the material parameters of end-point compounds, namely GaN and AlN, are taken from the literature, as shown in Table 1. The parameters for the alloys are assumed to obey the Vegard's law, and the bowing parameter for the bandgap energy of strain-free $Al_xGa_{1-x}N$ is chosen as 0.82 eV [41]. We use energy notations E_1, E_2, and E_3 hereafter, because the crystal symmetry of the $Al_xGa_{1-x}N$ films suffering from anisotropic stresses is no longer C^4_{6v}.

Table 1. Optical Constants of Thin Films of Materials[a]

	GaN[a]	AlN[b]
E_g at 10 K (eV)	3.504	6.095
$\Delta_{cr} = \Delta_1$ (meV)	16	–152.4
$\Delta_{so} = 3\Delta_2 = \Delta_3$ (meV)	22	18.9
$m^e_{//} / m_0$	0.2	0.32
$m^e_{\perp //} / m_0$	0.18	0.28
A_2	–0.91	–0.28
A_4	–2.83	–1.84
C_{11} (GPa)	390	396
C_{12} (GPa)	145	137
C_{13} (GPa)	106	120
D_1 (eV)	–41.4	–17.2
D_2 (eV)	–33.3	7.9
D_3 (eV)	8.2	8.19
D_4 (eV)	–4.1	–4.1
D_5 (eV)	–4.7	–3.4

[a]Reference 39.

[b]Reference 44.

The calculated relative oscillator strengths for the three interband transitions in the *m*-plane GaN are shown as functions of $\varepsilon_{X_1X_1}$ and $\varepsilon_{X_2X_2}$ by gray-scale contour plots in Fig. 5. For each E_1, E_2, and E_3 transition, the measured strain coordinate (strain-free) is plotted by a closed circle on the panel exhibiting the predominant polarization direction. As shown, the calculated polarization directions are X_1, X_3, and X_2 in order of decreasing electron energy. The result is consistent with previous studies on GaN [42,43]. Similar calculated results for the *m*-plane $Al_{0.03}Ga_{0.97}N$ are given in Fig. 6. For each E_1, E_2, and E_3 transition, the measured strain coordinate $\left(\varepsilon_{X_1X_1}, \varepsilon_{X_2X_2}\right) = \left(0.08\%, 0.13\%\right)$ is plotted by a closed circle on the panel exhibiting the calculated predominant polarization direction. Different from the case for GaN, the calculated polarization directions are X_3, X_1, and X_2 in order of decreasing electron energy. The result means that anisotropic strain induces a remarkable change in the electronic band structures. In the case of $Al_{0.70}Ga_{0.30}N$ alloy with $\left(\varepsilon_{X_1X_1}, \varepsilon_{X_2X_2}\right) = \left(0.79\%, 0.35\%\right)$, the

#149903 - $15.00 USD Received 24 Jun 2011; revised 29 Jun 2011; accepted 30 Jun 2011; published 1 Jul 2011

polarization directions are X_3, X_2, and X_1 in order of decreasing electron energy, as shown in Fig. 7. As revealed from Figs. 6 and 7, the polarization ordering of $Al_{0.70}Ga_{0.30}N$ was different from $Al_{0.03}Ga_{0.97}N$, and the oscillator strengths of $Al_{0.70}Ga_{0.30}N$ showed weaker contrast than those of GaN and $Al_{0.03}Ga_{0.97}N$. Similar results are found in the case of AlN, as shown in Fig. 8. The reason for this will be explained later. Gil and Alemu [23] have reported a theoretical study on the electronic band structure of *m*-plane GaN under anisotropic biaxial strain. They predicted that E_1 and E_3 transitions were $E \perp c$ (X_1) polarized under large in-plane compressive strain. With respect to E_3 transition, their result differs from our calculated result for AlGaN alloys suffering from biaxial compressive strain (data not shown in this paper, because our AlGaN films basically suffered from in-plane tensile strains). The discrepancy might arise from the fact that we did not consider the excitonic effects. However, it is likely that their notation was different [24] from ours so that their *m*-plane would correspond to *a*-plane in our case, which might be the cause for this discrepancy. Similar arguments have been given by Bhattacharyya *et al* [31].

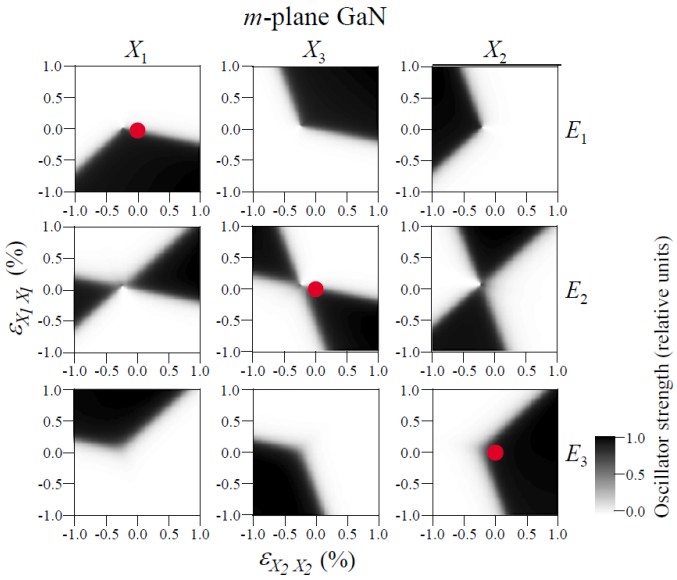

Fig. 5. Relative oscillator strengths of E_1, E_2, and E_3 transitions for the *m*-plane GaN film as functions of in-plane strain coordinate $\left(\varepsilon_{X_1X_1}, \varepsilon_{X_2X_2}\right)$. Closed circles indicate the experimentally obtained in-plane strain coordinate $\left(\varepsilon_{X_1X_1}, \varepsilon_{X_2X_2}\right) = (0.00\%, 0.00\%)$, which are plotted on the respective predominant polarization directions.

#149903 - $15.00 USD Received 24 Jun 2011; revised 29 Jun 2011; accepted 30 Jun 2011; published 1 Jul 2011

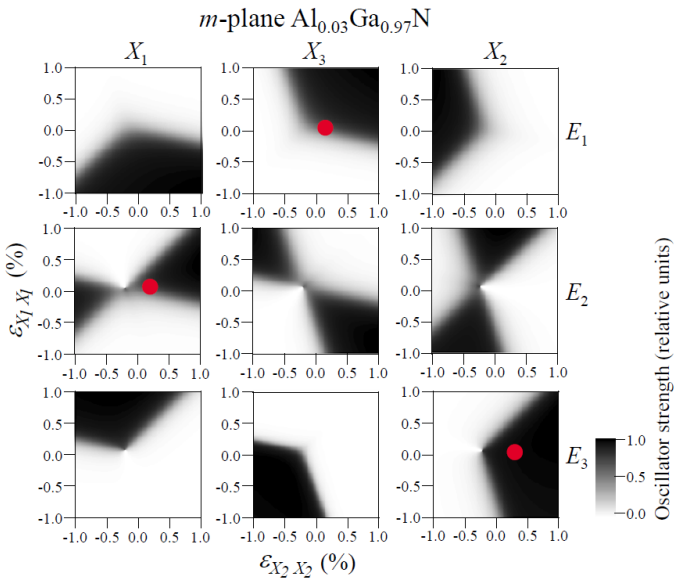

Fig. 6. Relative oscillator strengths of E_1, E_2, and E_3 transitions for the m-plane $Al_{0.03}Ga_{0.97}N$ film as functions of in-plane strain coordinate $\left(\varepsilon_{X_1X_1}, \varepsilon_{X_2X_2}\right)$. Closed circles indicate the experimentally obtained in-plane strain coordinate $\left(\varepsilon_{X_1X_1}, \varepsilon_{X_2X_2}\right) = (0.08\%, 0.13\%)$, which are plotted on the respective predominant polarization directions.

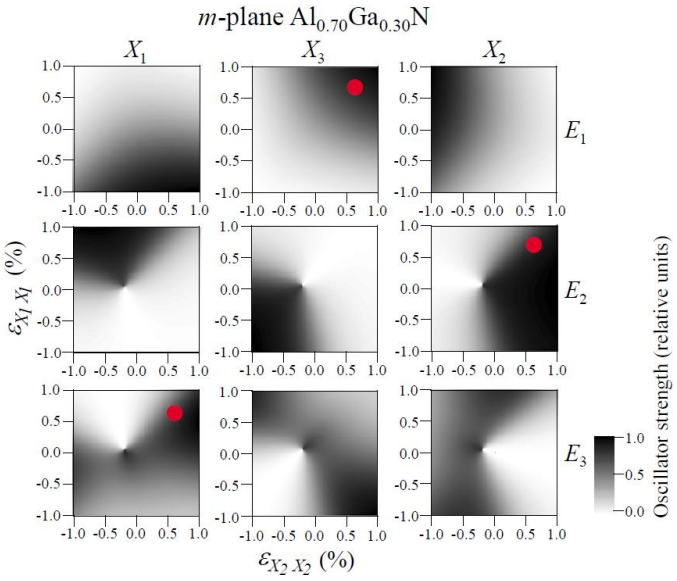

Fig. 7. Relative oscillator strengths of E_1, E_2, and E_3 transitions for the m-plane $Al_{0.70}Ga_{0.30}N$ film as functions of in-plane strain coordinate $\left(\varepsilon_{X_1X_1}, \varepsilon_{X_2X_2}\right)$. Closed circles indicate the experimentally obtained in-plane strain coordinate $\left(\varepsilon_{X_1X_1}, \varepsilon_{X_2X_2}\right) = (0.79\%, 0.35\%)$, which are plotted on the respective predominant polarization directions.

#149903 - $15.00 USD Received 24 Jun 2011; revised 29 Jun 2011; accepted 30 Jun 2011; published 1 Jul 2011

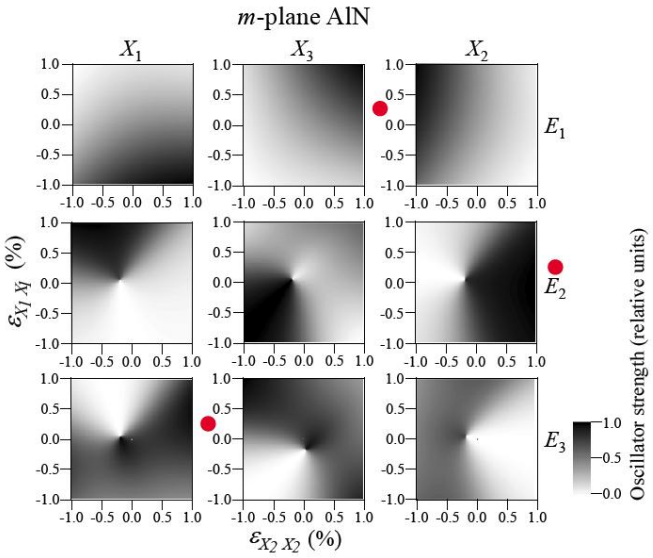

Fig. 8. Relative oscillator strengths of E_1, E_2, and E_3 transitions for the *m*-plane AlN film as functions of in-plane strain coordinate $\left(\varepsilon_{X_1X_1}, \varepsilon_{X_2X_2}\right)$. Closed circles indicate the experimentally obtained in-plane strain coordinate $\left(\varepsilon_{X_1X_1}, \varepsilon_{X_2X_2}\right) = (0.25\%, 1.96\%)$. They are plotted on the outside of the frameworks of respective predominant polarization directions.

The three exciton transition energies calculated for *m*-plane GaN, $Al_{0.03}Ga_{0.97}N$, $Al_{0.70}Ga_{0.30}N$, and AlN films under isotropic in-plane strain $\left(\varepsilon_{X_1X_1} = \varepsilon_{X_2X_2}\right)$ are shown in Figs. 9(a), 9(b), 9(c), and 9(d), respectively. In the case of GaN and $Al_{0.03}Ga_{0.97}N$, the VB anticrossing immediately takes place when in-plane biaxial tensile strain is introduced. On the contrary, the VB anticrossing gradually takes place with increasing the tensile strain for $Al_{0.70}Ga_{0.30}N$ and AlN. The latter result means that corresponding VBs are strongly hybridized, which gives rise to much lower oscillator strength contrast for $Al_{0.70}Ga_{0.30}N$ and AlN, as shown in Figs. 7 and 8. The energy differences between E_1 and E_2 bands for the GaN, $Al_{0.03}Ga_{0.97}N$, $Al_{0.70}Ga_{0.30}N$, and AlN films are shown as functions of $\varepsilon_{X_1X_1}$ and $\varepsilon_{X_2X_2}$ in Figs. 9(e), 9(f), 9(g), and 9(h), respectively, using contour lines. Similar to Figs. 5, 6, 7, and 8, the measured strain coordinates are plotted by closed black circles. The E_2-E_1 values, in the same order, are predicted to be 7.7 meV, 6.2 meV, 106 meV, and 142 meV.

Table 2 summarizes the polarization directions for the transitions and E_2-E_1 values calculated for *m*-plane $Al_xGa_{1-x}N$ suffering from the experimentally obtained strain values. As shown, E_1 transition is X_3-polarized regardless of *x*. The result means that E_1 (exciton) emission is essentially undetectable from the surface normal. Apart from E_1, the polarization directions alter from X_1 to X_2 for E_2 emission (X_3 to X_2 for E_3 emission) between $x = 0.25$ and 0.32. Assuming that the experimentally observed CL peaks principally originate from E_2 and E_3 transitions, the calculated prediction is consistent with the experimental results, as shown in Fig. 4(b). In Fig. 4(b), ρ values of *m*-plane $Al_xGa_{1-x}N$ films calculated using the oscillator strengths for the measured $\left(\varepsilon_{X_1X_1}, \varepsilon_{X_2X_2}\right)$ coordinates are plotted as a function of *x* by open circles. As shown, the experimental data nearly agree with the calculated ones, except rather low ρ values for $x \leq 0.25$. The low ρ values may be due to the light depolarization caused by high density surface striations along the *c*-axis, which had been disclosed using atomic force microscopy observation [33]. We must note in Fig. 4(a) that overall CL intensity for the samples of $x \geq 0.58$ is much weaker than that for $x \leq 0.32$. From Table 2, it is obvious that E_2-E_1 increases with *x*. Therefore, Boltzmann distribution gives rise to very low hole populations in

#149903 - $15.00 USD Received 24 Jun 2011; revised 29 Jun 2011; accepted 30 Jun 2011; published 1 Jul 2011

E_2 and E_3 bands in comparison with E_1 band for high x samples. This may be one of the reasons for the low CL intensities at low temperature, where nonradiative recombination channels are in principle frozen.

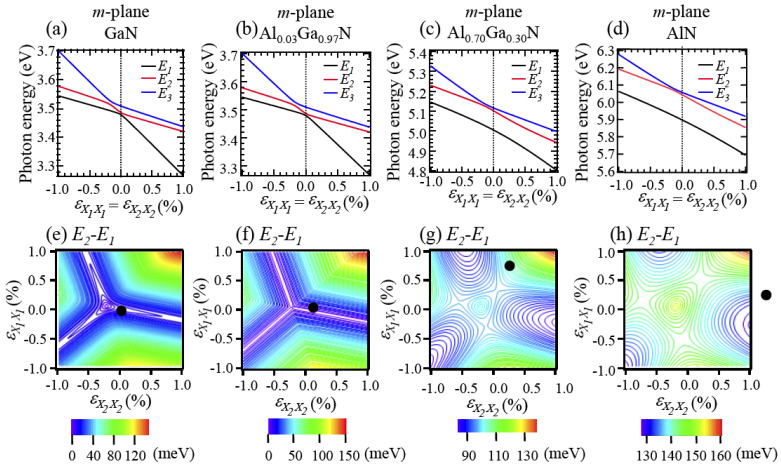

Fig. 9. Calculated E_1, E_2, and E_3 exciton transition energies for the m-plane (a) GaN, (b) $Al_{0.03}Ga_{0.97}N$, (c) $Al_{0.70}Ga_{0.30}N$, and (d) AlN films. The energy difference between E_2 and E_1, (E_2-E_1), as functions of in-plane strains $\left(\varepsilon_{X_1X_1}, \varepsilon_{X_2X_2}\right)$ for the m-plane (e) GaN, (f) $Al_{0.03}Ga_{0.97}N$, (g) $Al_{0.70}Ga_{0.30}N$, and (h) AlN films. Closed circles indicate respective in-plane strains.

Table 2. Calculated polarization directions for E_1, E_2, and E_3 transitions and energy differences between E_1 and E_2 band (E_2-E_1).

x	E_1	E_2	E_3	E_2-E_1 (eV)
0.00	X_1	X_3	X_2	7.7
0.03	X_3	X_1	X_2	6.2
0.12	X_3	X_1	X_2	48.4
0.25	X_3	X_1	X_2	96.9
0.32	X_3	X_2	X_1	124
0.58	X_3	X_2	X_1	88.4
0.70	X_3	X_2	X_1	106
0.73	X_3	X_2	X_1	108
1.00	X_3	X_2	X_1	142

Finally, calculated E_2 transition energies (closed squares), CL peak energies (open circles), and their energy differences (ΔE) for the m-plane $Al_xGa_{1-x}N$ films are plotted as a function of x in Fig. 10. The ΔE value, which is similar to the Stokes-type shift, ranges between 3 and 577 meV for the alloys. These values are slightly larger than those reported for c-plane AlGaN films grown by MOVPE (100 ~250 meV) [40], indicating the difficulties in growing homogeneous, excellent quality m-plane AlGaN epilayers. Leastwise, current m-plane $Al_xGa_{1-x}N$ films exhibit UV emission peaks between 360 nm (x = 0) and 210 nm (x = 1).

#149903 - $15.00 USD Received 24 Jun 2011; revised 29 Jun 2011; accepted 30 Jun 2011; published 1 Jul 2011

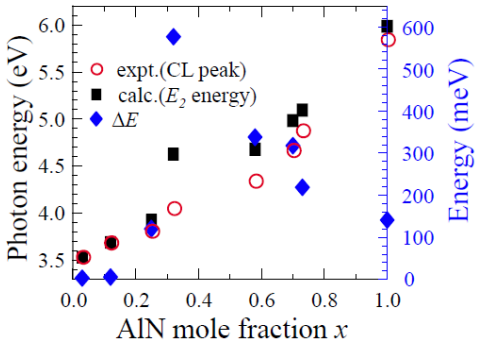

Fig. 10. Calculated E_2 transition energies (closed squares), measured CL peak energies (open circles), and their energy differences (closed diamonds) for the *m*-plane $Al_xGa_{1-x}N$ films as a function of *x*.

4. Conclusion

Interband optical polarization characteristics of UV-light-emitting *m*-plane $Al_xGa_{1-x}N$ alloy films grown on the *m*-plane FS-GaN substrates were interpreted by means of polarized CL measurements and theoretical calculations. The predominant light-polarization direction of the emission peak for the films suffering from in-plane anisotropic tensile stresses was shown to alter from $E\perp c$ (X_1) to $E//c$ (X_2) between x = 0.25 and 0.32. Theoretical analysis of the oscillator strengths of interband transitions and exciton transition energies was carried out using Bir-Pikus Hamiltonian, taking the anisotropic strain into account. The calculation predicted that the lowest energy transition (E_1) is X_3-polarized regardless of x, meaning that edge-emitting LED configuration is preferred for E_1 exciton emission. For surface-emitting configuration, the calculated polarization direction altered from X_1 ($E\perp c$) to X_2 ($E//c$) for E_2 transition and X_3 to X_2 for E_3 transition between x = 0.25 and 0.32. The variations of polarization ratio and overall CL intensity as a function of x were quantitatively reproduced through the calculation. These achievements may open the way of designing UV LEDs using nonpolar AlGaN alloys.

Acknowledgments

The authors would like to thank K. Fujito, H. Namita, T. Nagao, and H. Itoh of Mitsubishi Chemical Holdings Group for providing the *m*-plane FS-GaN substrates. They also would like to thank T. Hoshi, M. Kagaya, and Dr. T. Onuma for their help in the experiments. This work was supported in part by Grant-in-Aids of CANTech, IMRAM, Tohoku University, Scientific Research in Priority Area No. 18069001 under MEXT, NEDO program under METI, Japan, and AFOSR/AOARD Grant (FA2386-09-1-4013 and FA2386-10-1-4100) monitored by Dr. G. Jessen.

#149903 - $15.00 USD Received 24 Jun 2011; revised 29 Jun 2011; accepted 30 Jun 2011; published 1 Jul 2011

(2) Impacts of anisotropic tilt mosaics of state-of-the-art *m*-plane freestanding GaN substrates on the structural and luminescent properties of *m*-plane $Al_xGa_{1-x}N$ epilayers
-Journal of Vacuum Science and Technology B 29, 021208 (2011) attached in the next 9 pages-

Impacts of anisotropic tilt mosaics of state-of-the-art *m*-plane freestanding GaN substrates on the structural and luminescent properties of *m*-plane $Al_xGa_{1-x}N$ epilayers

K. Hazu,[a] M. Kagaya, T. Hoshi, T. Onuma, and S. F. Chichibu
CANTech, Institute of Multidisciplinary Research for Advanced Materials, Tohoku University, 2-1-1 Katahira, Aoba, Sendai 980-8577, Japan

(Received 6 September 2010; accepted 17 February 2011; published 16 March 2011)

Impacts of grown-in anisotropic tilt mosaics of state-of-the-art *m*-plane freestanding GaN (FS-GaN) substrates on the structural and luminescent properties of *m*-plane $Al_xGa_{1-x}N$ epilayers are described. The results of cross-sectional transmission-electron microscopy and transmission-electron diffraction analyses reveal the following plane defects formation, even in mostly pseudomorphic epilayers: (i) The formation of basal-plane stacking faults (BSFs) is hard to avoid in the case of lattice-mismatched $Al_xGa_{1-x}N$ thick film growth and (ii) the anisotropic greater *m*-plane tilt mosaic along the *a*-axis (twist in *c*-plane) of FS-GaN gives rise to pronounced formation of surface striations along the *c*-axis and planar-defect network (PDN) located on prismatic $\{10\bar{1}0\}$ planes and pyramidal $\{1\bar{1}0n\}$ planes, which are often terminated by BSF, especially in the case of the epilayers grown by NH_3-source molecular-beam epitaxy. These PDNs are assigned by spatially resolved cathodoluminescence (CL) and time-resolved photoluminescence measurements to associate with a characteristic emission peak approximately 200–300 meV lower than the near-band-edge (NBE) emission peak. Based on our database made with the aid of the positron-annihilation technique, three deep-state CL bands are correlated with cation vacancies (V_{III}) and cation-vacancy complexes. The intensity of the emission band originating from V_{III}-oxygen complexes was weaker by more than two orders of magnitude than the NBE peak. © *2011 American Vacuum Society.* [DOI: 10.1116/1.3566010]

I. INTRODUCTION

Wurtzite $Al_xGa_{1-x}N$ alloys are an outstanding candidate material for ultraviolet light-emitting diode (LED) and laser diode (LD) applications, as well as high-power high-frequency heterostructure field-effect transistors (HFETs). The spontaneous and piezoelectric polarization discontinuity at a Ga-polar *c*-plane $Al_xGa_{1-x}N$/GaN heterointerface results in immobile positive charge formation, which induces a two-dimensional electron gas (2DEG). The 2DEG concentration is as high as 10^{13} cm^{-2} in the ordinary AlGaN/GaN HFET structure.[1] However, the polarization-induced 2DEG simultaneously involves difficulties in operating HFETs in the enhancement mode (E-mode) that is desirable for power-switching devices. In addition, immobile charges of opposite signs formed at the opposite interfaces of quantum wells give rise to unwanted quantum-confined Stark effects,[2,3] which cause a poor overlap of electron and hole wave functions.

To get rid of polarization-discontinuity problems, the use of nonpolar[4] and semipolar[5] planes has attracted attention,[6] because heterointerfaces formed on off-polar planes have less *net* polarization-discontinuity charges.[7] Similar to the success in fabricating excellent performance *m*-plane InGaN blue LEDs,[8] LDs,[9,10] and $(20\bar{2}1)$ plane green LDs,[11,12] the use of low-defect-density *m*-plane freestanding GaN (FS-GaN) substrates[13] sliced from a *c*-plane FS-GaN boule grown by halide-vapor phase epitaxy (HVPE) has enabled fabricating an E-mode (normally off) *m*-plane AlGaN/GaN HFET.[14] However, because the state-of-the-art *m*-plane FS-GaN (Ref. 13) is prepared by slicing nearly 1-cm-thick *c*-plane FS-GaN grown in Ga-polar [0001] direction, the *c*-plane tilt (including the wafer bowing) and twist mosaics of the initial crystal are transferred to blurring of the *c*-axis and the greater *m*-plane tilt mosaic along the *a*-axis, respectively, as shown schematically in Figs. 1(a) and 1(b). These anisotropic mosaics of the substrate *m*-plane would cause unwanted generation of extra defects, especially in lattice-mismatched alloy epilayers.

Despite such a circumstance, precise investigations of the structural and point defects have not been carried out on *m*-plane $Al_xGa_{1-x}N$ epilayers grown on either *m*-plane FS-GaN or other heteroepitaxial substrates, although they would limit[15,16] the performance and reliability of devices. For example, the authors have examined the impacts of anisotropic lattice relaxation on the crystal mosaicity of *m*-plane $Al_xGa_{1-x}N$ epilayers grown by ammonia-source molecular-beam epitaxy[17] (NH_3-MBE) on *m*-plane FS-GaN (Ref. 13) and found that the *m*-plane tilt mosaic along the *c*-axis is the same as the substrate as long as coherent growth was maintained. However, it became more severe than along the *a*-axis in lattice-relaxed films.[17] Therefore, it is worth correlating structural and point defects responsible for character-

[a]Author to whom correspondence should be addressed; electronic mail: chichibulab@yahoo.co.jp

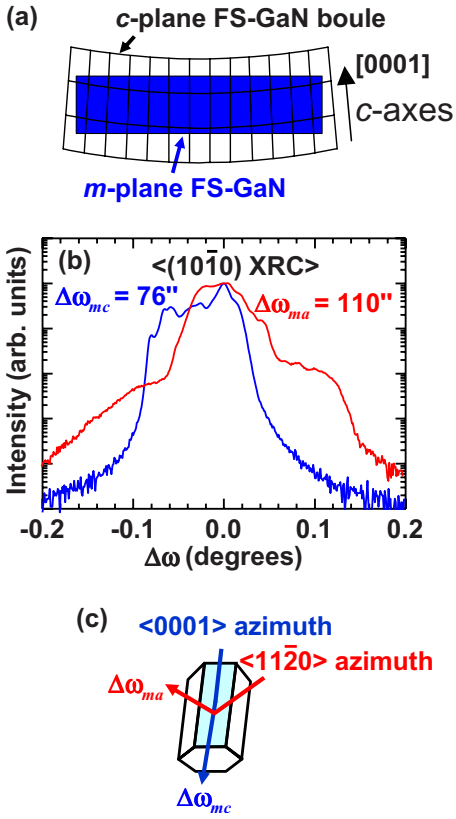

FIG. 1. (Color online) (a) Schematic drawing of a *c*-plane FS-GaN boule grown on a *c*-plane Al_2O_3 substrate by HVPE and a sliced *m*-plane FS-GaN. (b) X-ray rocking curves for the (10$\bar{1}$0) diffraction of the *m*-plane FS-GaN. The x rays were irradiated along the *c*-axis or *a*-axis, as shown in (c).

istic luminescence peaks in *m*-plane $Al_xGa_{1-x}N$ films with particular structural imperfections generated in a state-of-the-art *m*-plane FS-GaN substrate.[13]

In this article, the results of wide-area and spatially resolved cathodoluminescence (CL) measurements, as well as those of time-resolved photoluminescence (TRPL) measurements on *m*-plane $Al_xGa_{1-x}N$ epilayers, are systematically compared with the results of x-ray diffraction (XRD) and transmission-electron microscopy (TEM) analyses to show how anisotropic tilt mosaics of the *m*-plane FS-GaN (Ref. 13) affect the structural and optical properties of $Al_xGa_{1-x}N$ overlayers. Even though FS-GaN was used, the formation of basal-plane stacking faults (BSFs) was hard to avoid in the case of lattice-mismatched thick $Al_xGa_{1-x}N$ film growth. In addition, TEM and transmission-electron diffraction (TED) analyses reveal that anisotropic greater *m*-plane tilt mosaic along the *a*-axis of FS-GaN gave rise to pronounced formation of planar-defect networks (PDNs) located on prismatic {10$\bar{1}$0} planes and pyramidal {1$\bar{1}$0*n*} planes. The PDNs are visualized using spatially resolved cathodoluminescence (SRCL) measurement to associate with the characteristic CL peak approximately 200–300 meV lower in energy than the near-band-edge (NBE) emission peak. The low-temperature photoluminescence (PL) lifetime (τ_{PL}) for the peak assigned to associate with BSFs was longer than the NBE peak. Finally, the importance of decreasing point-defect concentrations, such as group-III vacancies (V_{III}), unnecessary, and their complexes is suggested.

II. EXPERIMENT

Because the molecular-beam epitaxy (MBE) method in general has an advantage in obtaining abrupt semiconductor heterointerfaces, both NH_3-MBE (Ref. 17) and metalorganic vapor-phase epitaxy (MOVPE) were used for the epitaxial growth. After growing a 1-μm-thick GaN homoepitaxial base layer, approximately 100- to 400-nm-thick *m*-plane $Al_xGa_{1-x}N$ films were grown on a 325-μm-thick *m*-plane FS-GaN.[13] The surface of as-received substrates was inspected by atomic-force microscopy (AFM) and found to have smooth morphology with monolayer atomic steps.[13,17,18] However, the x-ray rocking curves (XRCs) exhibited multiple-peak or asymmetric line shapes,[17] as shown in Fig. 1(b). This multiple grain structure principally originates from the bowing of the original *c*-plane FS-GaN, as already explained in Fig. 1(a).[13] For instance, the values of full width at half-maximum (FWHM) of XRCs for the present substrate were $\Delta\omega_{mc}=76$ and $\Delta\omega_{ma}=110$ arc sec for the (10$\bar{1}$0) diffraction along ⟨0001⟩ and ⟨11$\bar{2}$0⟩ azimuths, respectively, and $\Delta\omega_r=100$ arc sec for the (10$\bar{1}$2) diffraction [Fig. 1(b)]. Threading dislocations (TDs) and BSFs were unseen by TEM in the GaN homoepitaxial base layers: The TD and BSF densities were lower than 5×10^6 cm^{-2} and 1×10^3 cm^{-1}, respectively.[17,18]

The $Al_xGa_{1-x}N$ growth by NH_3-MBE was carried out at the growth temperature (T_g) between 870 and 970 °C using 99.999 99%-pure Al and Ga metals and a purified NH_3 gas.[17] Trimethylaluminium, trimethylgallium, and a purified NH_3 gas were used for MOVPE. T_g was kept below 1120 °C to prevent the FS-GaN from decomposing.

High-resolution XRD measurements were carried out using a four-crystal monochromator and an analyzer crystal (Bruker D8). A system with a one-dimensional detector array was used to obtain the x-ray reciprocal space mapping (X-RSM) images. Macroarea CL (560 $\mu m\phi$) was excited with an electron beam (EB) operated at 3.0 kV with the emission current density of 1.0×10^{-2} A/cm^2 at sample. Microarea CL (1.0×2.2 μm^2) and SRCL (a few nmϕ) were excited using an EB with or without beam scanning and were dispersed using a 20-cm-focal-length grating monochromator equipped on a scanning-electron microscope (SEM). The acceleration voltage and current of EB were typically 5 kV and 500 pA, respectively. Monochromatic SRCL intensity images were taken at the wavelengths of interest with the beam scanning at 295 K. TRPL was excited using a frequency-tripled or frequency-quadrupled mode-locked Al_2O_3:Ti laser at 8 K. The pulse width, repetition rate, and power density were ~100 fs, 80 MHz, and 120 nJ/cm^2 per pulse, respectively. A pulse picker was used for the samples exhibiting τ_{PL} longer than 12 ns to reduce the repetition rate of the excitation pulses. The TRPL signal was acquired using a streak camera.

III. RESULTS AND DISCUSSION

A. Structural features

The *m*-plane $Al_xGa_{1-x}N$ epilayers of low AlN mole fraction x ($0<x\leq 0.32$) were confirmed by X-RSM to grow coherently on the GaN base layers. Other high AlN mole fraction epilayers ($x\geq 0.35$) were partially or nearly fully relaxed. Due to the tensile strain, the epilayers of $x\geq 0.35$ had macroscopic surface cracks. Representative X-RSM images for the pseudomorphic $Al_{0.25}Ga_{0.75}N$ and mostly relaxed $Al_{0.70}Ga_{0.30}N$ epilayers grown by NH_3-MBE are displayed in Fig. 2. In each panel, the ideal location for strain-free AlN is shown by a closed (red) circle for comparison. We note that critical layer thicknesses calculated by the model given by People and Bean[19] are 202 nm for $x=0.25$ and 31 nm for $x=0.52$, taking in-plane anisotropic lattice and thermal-expansion mismatches into account. Because both the pseudomorphic and relaxed films suffered from anisotropic strains, x values were calculated from the out-of-plane (*m*-axis) and in-plane (*c*- and *a*-axes) lattice parameters, which were obtained from a 2θ-ω scan for the $(10\bar{1}0)$ XRD and X-RSM results for $(2\bar{2}01)$ and $(1\bar{3}20)$ diffractions, respectively (see Fig. 2, for example). The relation $\epsilon_{X_3X_3}=(-C_{12}\epsilon_{X_1X_1}-C_{13})/C_{11}$ was used, where $\epsilon_{X_3X_3}$, $\epsilon_{X_1X_1}$, and $\epsilon_{X_2X_2}$ are the strains along *m*-, *a*-, and *c*-axes and C_{ij} are the elastic stiffness constants. In the calculation,[17] elastic stiffness constants of $Al_xGa_{1-x}N$ alloys were assumed to obey[20] Vegard's law.

Representative surface AFM images of approximately 60- to 100-nm-thick pseudomorphic *m*-plane $Al_xGa_{1-x}N$ epilayers grown by MOVPE ($x=0.17$) and NH_3-MBE ($x=0.25$) are shown in Fig. 3. The surface of the MOVPE epilayer exhibits well-aligned 0.26-nm-high *monolayer* atomic step lines, as shown in Fig. 3(a). Conversely, the MBE epilayer exhibits surface striations parallel to the *c*-axis. We note that the striations have already been formed during the underlayer GaN growth.[17] Therefore, different from the MOVPE case, it seems difficult for NH_3-MBE (Refs. 17 and 21) to eliminate such striations, even for the binary GaN growth. The reason for this may be an inappropriate surface preparation or insufficient migration of Ga adatoms due to lower T_g in comparison with MOVPE, because NH_3-MBE is a surface-sensitive growth method. Indeed, the depth of the striations in the $Al_xGa_{1-x}N$ films was deeper than the GaN case, where Al-containing materials need higher T_g to ensure sufficient surface migration. Here, we note that the in-plane polar direction of the epilayer was confirmed by convergent-beam electron diffraction (CBED) measurement to be the same as the substrate.

Despite the presence of such surface striations, all the *m*-plane $Al_xGa_{1-x}N$ films grown by NH_3-MBE exhibit a single $(10\bar{1}0)$ XRD peak, similar to the case for the MOVPE films. The results mean that both the MOVPE/MBE epilayers did not show noticeable phase separation or compositional ordering along the *m*-axis. However, similar to FS-GaN, XRCs for the pseudomorphic $Al_xGa_{1-x}N$ films exhibit a multiple-peak or asymmetric line shape, as shown in Fig.

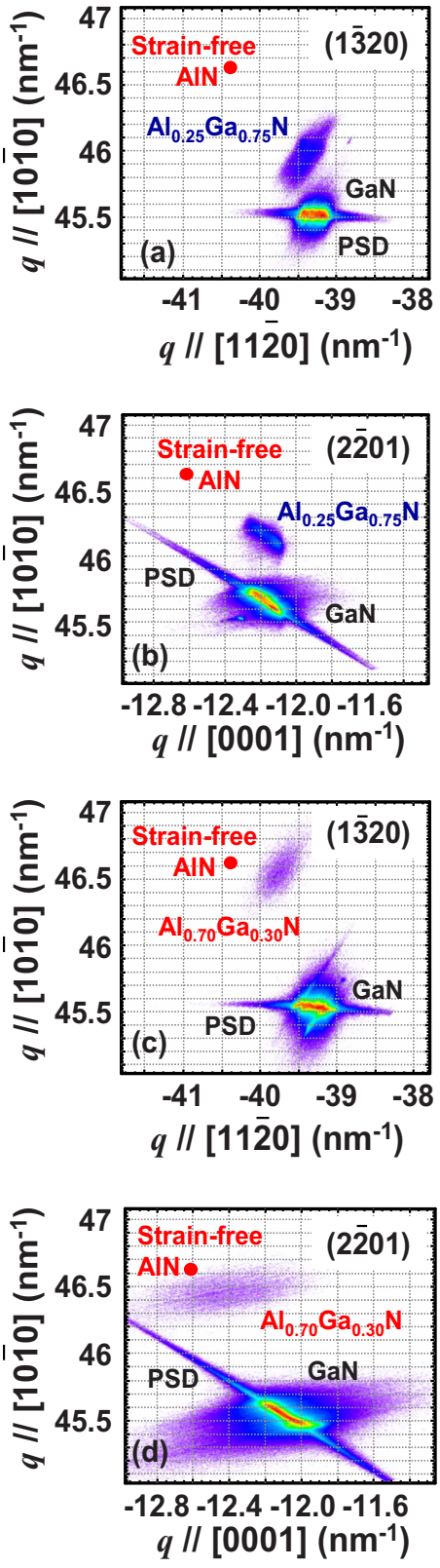

FIG. 2. (Color online) Representative X-RSM images for the pseudomorphic *m*-plane $Al_{0.25}Ga_{0.75}N$ epilayer grown on the *m*-plane FS-GaN taken in the vicinity of (a) $(1\bar{3}20)$ and (b) $(2\bar{2}01)$ diffraction spots. The images show partially lattice-relaxed $Al_{0.70}Ga_{0.30}N$ epilayer taken for (c) $(1\bar{3}20)$ and (d) $(2\bar{2}01)$ diffractions. Both the epilayers were grown by NH_3-MBE. The closed circle in each panel shows the ideal location of strain-free AlN, for comparison.

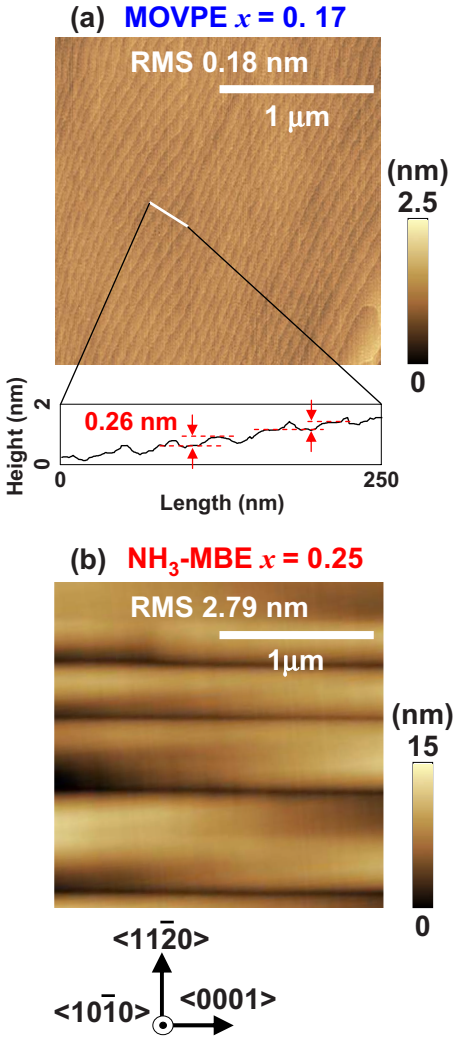

FIG. 3. (Color online) Representative surface AFM images for (a) a 60-nm-thick *m*-plane $Al_{0.17}Ga_{0.83}N$ epilayer grown by MOVPE and (b) 120-nm-thick *m*-plane $Al_{0.25}Ga_{0.75}N$ epilayer grown by NH_3-MBE. Both the epilayers were coherently grown on the *m*-plane FS-GaN. Cross-sectional height profile for the MOVPE epilayer is also shown in (a) for clarity.

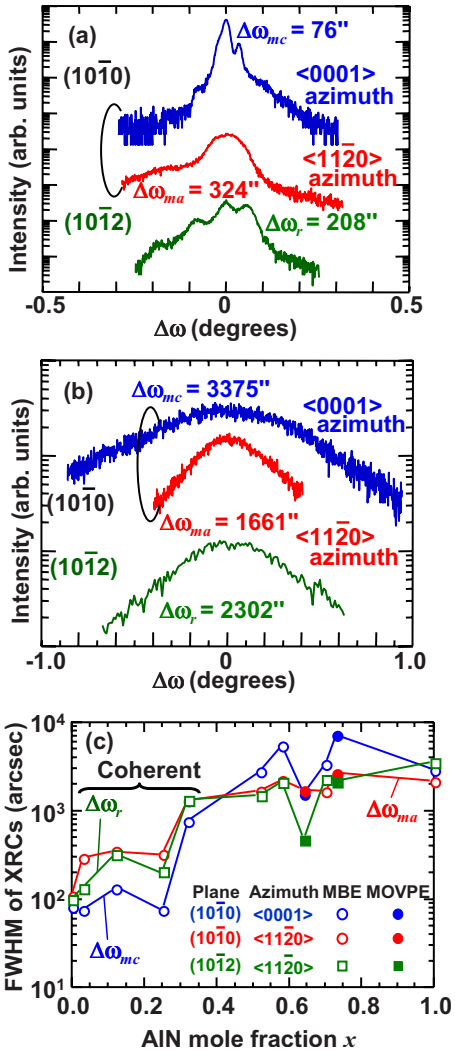

FIG. 4. (Color online) Representative XRCs taken for (10$\bar{1}$0) and (10$\bar{1}$2) diffractions of (a) pseudomorphic *m*-plane $Al_{0.25}Ga_{0.75}N$ and (b) mostly relaxed *m*-plane $Al_{0.70}Ga_{0.30}N$ epilayers grown by NH_3-MBE. (c) FWHM values for the XRCs ($\Delta\omega_{mc}$, $\Delta\omega_{ma}$, and $\Delta\omega_r$) of *m*-plane $Al_xGa_{1-x}N$ epilayers grown by NH_3-MBE and MOVPE.

4(a), for example (x=0.25). Because this is also the case for both underlying GaN homoepitaxial films[18,22] and the substrate,[13] the multidomain structure (bowing) of the original *c*-plane FS-GaN must be the major reason [see Fig. 1(a)]. In contrast, relaxed $Al_xGa_{1-x}N$ films exhibit broad but single-peaked XRCs, as shown in Fig. 4(b), for example (x=0.70). In those films, the multiple domain fine structure seems to be hidden due to the broadness of the line shape.

As long as coherent growth was maintained, $\Delta\omega_{mc}$ of the $Al_xGa_{1-x}N$ epilayers are the same as the substrate regardless of the presence of striations, as shown in Fig. 4(c). The result is similar to the case with pseudomorphic *m*-plane $In_xGa_{1-x}N$ ($x \leq 0.14$) epilayers[22] grown on the *m*-plane FS-GaN prepared by the same provider (Mitsubishi Chemical Corporation). However, $\Delta\omega_{ma}$ and $\Delta\omega_r$ immediately increased for $0 < x \leq 0.25$, presumably because the twist mosaic along the *c*-axis of the initial *c*-plane FS-GaN was exaggerated by the lattice and thermal-expansion mismatches between AlGaN and GaN during "surface-sensitive" NH_3-MBE. This must be another origin for the deeper striations in the $Al_xGa_{1-x}N$ films, in comparison with GaN films. The broader horizontal width of the (1$\bar{3}$20) X-RSM spot for the $Al_{0.25}Ga_{0.75}N$ epilayer [Fig. 2(a)] also reflects the result. For the $Al_{0.32}Ga_{0.68}N$ film, $\Delta\omega$ values were larger than those for $x \leq 0.25$, reflecting the increase in misfit dislocation densities.

Even for the pseudomorphic *m*-plane $Al_xGa_{1-x}N$ films, the formation of planar defects, such as stacking faults, was hard to avoid, as follows. Cross-sectional TEM and TED images taken along the ⟨11$\bar{2}$0⟩ and ⟨0001⟩ EB azimuths for the $Al_{0.25}Ga_{0.75}N$ epilayer grown by NH_3-MBE are summarized in Fig. 5. From the number of visible BSFs marked by black/white arrows in Fig. 5(a), the BSF density in the $Al_{0.25}Ga_{0.75}N$ layer is estimated to be as high as 10^6 cm^{-2}. This value is more than three orders of magnitude higher than the substrate (and the GaN epilayer). The horizontal

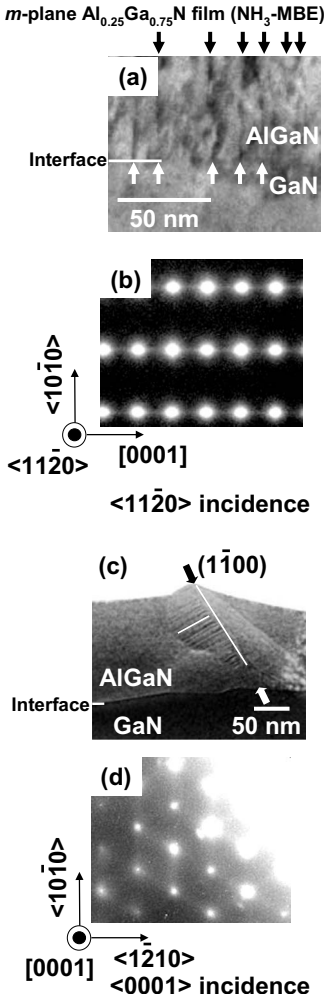

FIG. 5. (a) Cross-sectional TEM image and (b) TED pattern for the *m*-plane $Al_{0.25}Ga_{0.75}N$ epilayer grown by NH_3-MBE taken with the EB incidence along the *a*-axis. (c) and (d) show the same data set taken with EB incidence along the *c*-axis. Streak lines connecting the diffraction spots in TED patterns (b) and (d) are due to the presence of planar defects such as BSFs on {0001} planes and SMBs on prismatic {10$\bar{1}$0} planes, respectively.

streak lines connecting the TED spots in Fig. 5(b) indicate the presence of planar defects, such as BSFs and twins, on *c*-planes. Apparently from Fig. 5(a), BSFs are generated at the $Al_{0.25}Ga_{0.75}N/GaN$ interface due to the lattice mismatch. However, the X-RSM image indicates that the *c*-axis length of the $Al_{0.25}Ga_{0.75}N$ epilayer is the same as the GaN value. Therefore, the insertion of extra planes might decelerate the lattice relaxation along the *c*-axis. On the other hand, the *a*-axis length for the same epilayer is a little bit shorter than the GaN, as shown in Fig. 2(a), indicating the precursor of lattice relaxation.

In addition to BSFs, high-density PDNs were found right underneath the ridges, which are mostly formed along with the surface striations, as shown in Fig. 5(c). The rhombic streak lines connecting the TED spots in Fig. 5(d) indicate the presence of planar faults, such as twins or atom displacements, in prismatic {10$\bar{1}$0} planes and possibly {1$\bar{1}$0*n*} *tilted* *m*-planes (so-called *r*-planes). However, noticeable planar defects are not observed on prismatic {11$\bar{2}$0} *a*-planes, as shown in Figs. 5(c) and 5(d). The result indicates that *a*-plane prismatic stacking faults[23,24] (PSFs) are not formed in the present films. On prismatic {10$\bar{1}$0} *m*-planes, two types of defects are known to appear in wurtzite GaN.[25] They are inversion-domain boundaries (IDBs) and stacking-mismatch boundaries (SMBs).[26] Because the CBED results for the $Al_{0.25}Ga_{0.75}N$ epilayer and the GaN base layer indicated no change in the polarity, IDBs were not formed in our experiment. Neumann *et al.*[25] pointed out that SMBs could be formed on prismatic {10$\bar{1}$0} planes in the *m*-plane GaN epilayer grown on the (100) γ-$LiAlO_2$ substrate. Here, SMBs do not introduce an inversion into the crystal, but introduce a shift into the structure along the [0001] GaN direction and can be terminated by BSF. Here, we note that SMBs on prismatic {10$\bar{1}$0} planes will appear at the edge (line) along the *c*-axis in the (10$\bar{1}$0) *m*-plane surface. The influences of these BSFs and PDNs on the optical properties will be discussed later.

In contrast to pseudomorphic epilayers, $\Delta\omega_{mc}$ became larger than $\Delta\omega_{ma}$ or $\Delta\omega_r$ for the relaxed $Al_xGa_{1-x}N$ epilayers ($x \geq 0.52$), as shown in Figs. 2(c), 2(d), 4(b), and 4(c). In these relaxed films, the presence of high-density BSFs was obvious. In addition, as the growth rates toward the (Al,Ga)-polar and N-polar directions are different,[27] asymmetric coalescence may disturb the lattice coherence.[28] Indeed, segmented surface morphology was observed for the $Al_{0.70}Ga_{0.30}N$ epilayer.[17] It should be noted that lattice and thermal-expansion mismatches along the *c*-axis are larger than along the *a*-axis for *m*-plane $Al_xGa_{1-x}N/GaN$ heterostructures. Interestingly, however, the X-RSM measurement revealed that lattice relaxation along the *a*-axis took place faster than along the *c*-axis for $0.52 \leq x \leq 0.7$. This phenomenon can be interpreted[17,25] due to the grown-in larger *m*-plane tilt mosaic along the *a*-axis of FS-GaN [see Fig. 1(a)],[18] which generates the inclined prismatic (10$\bar{1}$0) planar defects and stacked planar faults terminated by the SMB, as shown in Fig. 5(c).

B. Luminescence spectra and origins of the emissions

Unpolarized macroarea CL spectra for the *m*-plane $Al_xGa_{1-x}N$ epilayers measured at 8–12 K are summarized in Fig. 6. They typically exhibit a NBE emission band that contained two or three components. They are the highest emission-energy peak or shoulder labeled P1 (marked by circles) and one or two peaks labeled P2 and P3 that are approximately 100–300 meV lower in energy than P1 and marked by diamonds and rectangles, respectively. Also, the considerably weak two or three broad emission bands labeled B4, B5, and B6 were found, which originate from deep states. Their peak energies are plotted as functions of x in Fig. 7. For comparison, the band gap energy (E_g) of nearly strain-free *c*-plane $Al_xGa_{1-x}N$ epilayers expressed by $E_g(x) = 6.095x + 3.504(1-x) - 0.82x(1-x)$ eV (Ref. 29) and the

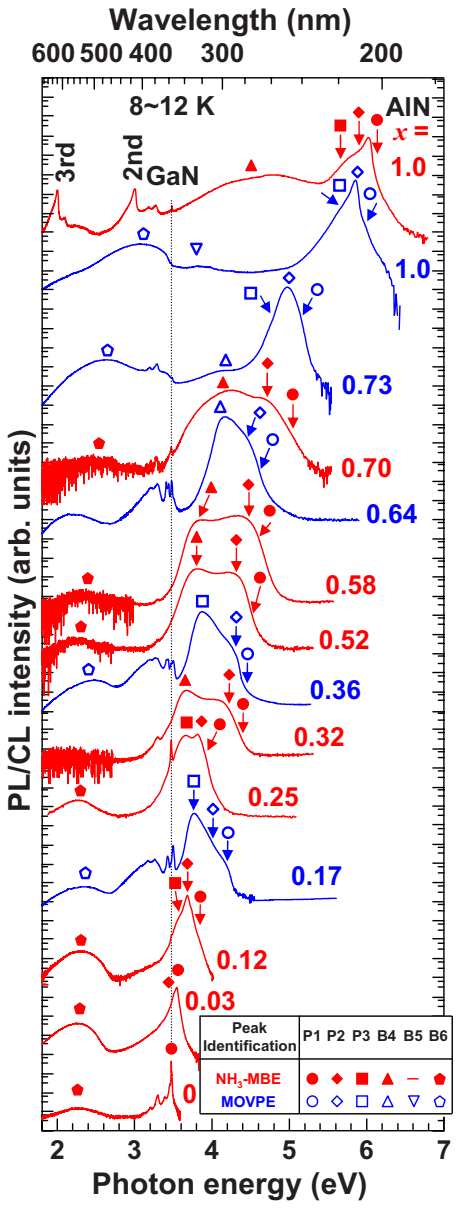

FIG. 6. (Color online) (a) Unpolarized macroarea (560 $\mu m\phi$) CL spectra for the *m*-plane $Al_xGa_{1-x}N$ epilayers measured at 8–12 K. Open and closed characters represent the identifications of peaks (P1, P2, and P3) and bands (B4, B5, and B6) in the epilayers grown by MOVPE and NH_3-MBE, respectively. The structures labeled 2nd and 3rd on the topmost trace are due to the higher order diffractions of the grating for the NBE peak.

NBE CL peak energy of zinc blende (ZB) cubic $Al_xGa_{1-x}N$ epilayers[30] are shown by a solid curve and a curve with hexagons, respectively.

The highest-energy P1 (circles) is assigned to free, bound, or localized excitonic emission, because the energy nearly agrees with the NBE emission for *c*-plane $Al_xGa_{1-x}N$ epilayers.[29] Because the energy difference between the excitonic emissions (3.47–3.48 eV) and the emission associated with BSFs (3.41 eV) (Refs. 31 and 32) in GaN have been quantified to be 60–70 meV and the CL peak energy of the NBE emission in ZB AlN (hexagon) was lower by 210 meV than the wurtzite AlN (Ref. 30), P2 (diamonds) is assigned to the emission associated with BSFs. Details of this assignment are discussed with the results of SRCL and TRPL measurements later. As a matter of fact, the BSF density in the particular *m*-plane $Al_{0.25}Ga_{0.75}N$ epilayer grown by NH_3-MBE was as high as 10^6 cm^{-2}, as shown in Fig. 5(a). The result means that the BSF spacing is as short as 10 nm and almost all excited carriers/excitons will be trapped by BSFs in such a portion having high-density BSFs. Therefore, in particular for the NH_3-MBE $Al_{0.25}Ga_{0.75}N$ film, a weak shoulder at around 3.9 eV (P1) is assigned to a localized or bound-type excitonic emission and the peak at 3.81 eV (P2) is assigned to associate with BSFs.

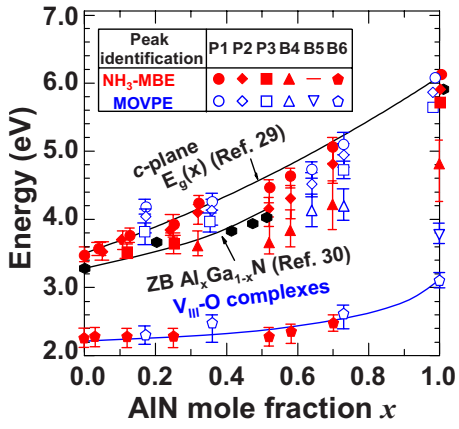

FIG. 7. (Color online) Energies of the CL peaks and bands as functions of *x*. For comparison, E_g of nearly strain-free *c*-plane $Al_xGa_{1-x}N$ epilayers (Ref. 29) (solid line) and CL peak energies of the ZB cubic $Al_xGa_{1-x}N$ epilayers (Ref. 30) (closed hexagons) are also shown.

In order to assign the origin of P3 (rectangles in Figs. 6 and 7), SRCL measurements were carried out for the samples of $x=0.25$, 0.36, 0.70, 0.73, and 1. The representative results at 293 K for the $Al_{0.25}Ga_{0.75}N$ epilayer grown by NH_3-MBE are summarized in Fig. 8. A remarkable double peak in the macroarea CL spectrum [Fig. 8(a)] and a broadband in the microarea scanning CL spectrum [Fig. 8(b)] were resolved to consist of two dominant discrete peaks P2 and P3, as shown in Fig. 8(c). In reality, very weak P1 existed as a higher energy shoulder. As shown, spot-excitation local CL spectra [Fig. 8(c)] measured at positions 1–3 [marked on the SEM image in Fig. 8(d)] exhibited P2, while the spectra for positions 4–6 exhibited both P2 and P3. As shown in Fig. 8(e), a monochromatic CL intensity image taken at 3.81 eV (P2) is nearly uniform, meaning that the photons were emitted from nearly entire areas. The result is consistent with the assignment given in the preceding paragraph; the average lateral BSF spacing along the *c*-axis was as short as 10 nm. We note that in Figs. 8(e)–8(g), the brightness of the images represents the relative CL intensity at each pixel: White areas correspond to the areas emitting stronger lights under study. In contrast to P2, the intensity image taken at 3.60 eV (P3) exhibits bright straight lines along the *c*-axis and triangular areas, as shown in Fig. 8(f). These characteristic emission patterns are found in very wide areas, as shown in the contracted CL intensity image for P3 in Fig. 8(g). The line locations correspond to the morphological ridges along the *c*-axis, as shown in Figs. 8(d) and 8(f). The triangular areas

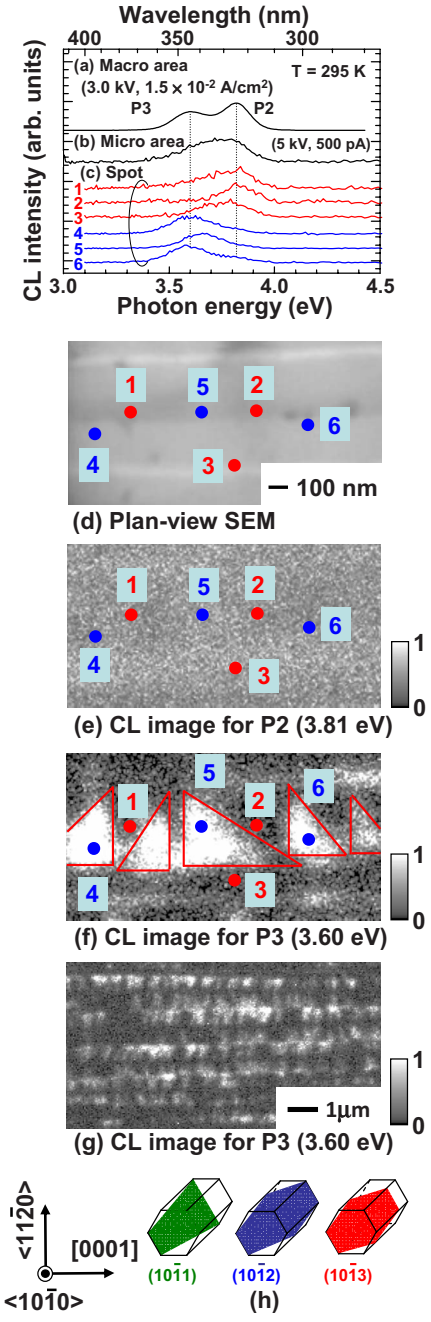

FIG. 8. (Color online) Room temperature (a) macroarea (560 $\mu m\phi$), (b) microarea (1.0×2.2 μm^2), and (c) spot-excitation local CL spectra for the *m*-plane $Al_{0.25}Ga_{0.75}N$ epilayer grown by NH_3-MBE. (d) Its plan-view SEM image shows the local excitation spots 1–6. Monochromatic CL intensity images monitored at (e) 3.81 eV (BSF peak P2). (f) and (g) show the CL intensity images monitored at 3.60 eV (PDN peak P3) taken for two magnifications. Brightness of the images represents relative CL intensity at each position. White areas correspond to the areas emitting stronger lights under study. (h) Schematic drawings of pyramidal $\{1\bar{1}0n\}$ planes ($n=1-3$), where the areas emitting P3 are localized.

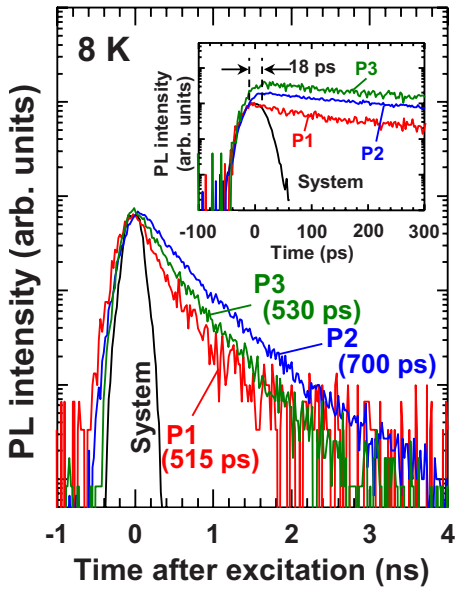

FIG. 9. (Color online) Energy-resolved low-temperature TRPL signals taken for P1, P2, and P3 of the *m*-plane $Al_{0.25}Ga_{0.75}N$ epilayer grown by NH_3-MBE. The peak energies and PL lifetimes (τ_{PL}) were 3.98 eV and 515 ps for P1 (NBE), 3.85 eV and 700 ps for P2 (BSFs), and 3.65 eV and 530 ps for P3 (PDNs). The inset shows the initial TRPL responses ($t\leq300$ ps). The peaks P2 and P3 exhibit noticeable delays of approximately 18 ps for the emission onset.

are seen from the sample surface as being surrounded by {0001} *c*-plane, *c*-axis, and certain axes inclined by quantized angles from the *a*-axis, as shown by solid triangles in Fig. 8(f). Because some of the areas (positions 4–6, for example) emit both P2 and P3, the areas emitting P3 are localized both laterally (in plane) and vertically (out-of-plane). Liu *et al.*[32] found spatially localized emissions at 3.41, 3.33, and 3.29 eV in *a*-plane GaN, which have been assigned to associate with BSFs, $\{11\bar{2}0\}$ *a*-plane PSFs intersecting BSFs, and partial dislocations terminating BSFs, respectively. However, as our samples do not have *a*-plane PSFs, as shown in Figs. 5(c) and 5(d), P3 is attributable to associate with PDNs, such as SMBs located on a prismatic $(10\bar{1}0)$ plane for the CL line along the *c*-axis in Fig. 8(f) and pyramidal $\{1\bar{1}0n\}$ planes for the triangular-shaped CL patterns in Fig. 8(f), where *n* values vary from 1 to 3, as shown schematically in Fig. 8(h). We note that the stacked planar defects shown in Fig. 5(c) may be inclined from the *c*-plane cross section and are on pyramidal $\{1\bar{1}0n\}$ planes, which can give rise to oblique CL intensity boundaries seen in Fig. 8(f). We also note that SMBs can be terminated by BSFs, giving the CL intensity boundary normal to the *c*-axis. Similar pyramidal plane-based stacking defects have been found by several groups.[25,33]

With respect to the recombination dynamics of the emission associated with BSFs, Corfdir *et al.*[34] observed longer low temperature (radiative) τ_{PL} for the peak at 3.41 eV (780 ps), in comparison with the donor-bound exciton peak in GaN ($\tau_{PL}\sim210$ ps). They also observed a significant delay in the rise time for the BSF peak up to 120 ps. In Fig. 9, energy-resolved TRPL signals taken for P1, P2, and P3 of the same *m*-plane $Al_{0.25}Ga_{0.75}N$ epilayer are displayed. As shown, TRPL signals for P2 and P3 show longer decay curves than P1. Their τ_{PL} values at 8 K were 515, 700, and 530 ps for P1, P2, and P3, respectively. In addition, P2 and P3 show a delay in the intensity rise, as shown in the inset. The time delays were approximately 18 ps in our case, which

was much shorter than the GaN case (120 ps) in Ref. 34. As the BSF density in the overgrown GaN wing region in Ref. 34 was much lower than ours, the difference is attributable to the carrier-transportation time. The result that τ_{PL} of P2 (700 ps) was longer than the P1 value is consistent with the result for GaN,[34] meaning that excitons localized in BSFs may take a long time to recombine, even in $Al_xGa_{1-x}N$ for x at least smaller than 0.25. Needless to say, relatively long τ_{PL} for P1 (515 ps) is consistent with the fact that excitons are localized in $Al_xGa_{1-x}N$ alloys. For example, τ_{PL} at 8 K for *c*-plane $Al_xGa_{1-x}N$ films was 360 ps for $x=0.11$ and 960 ps for $x=0.35$.[29] Different from the BSF peak P2, τ_{PL} of P3 was 530 ps at 8 K, which was just slightly longer than P1 (515 ps). Because SMBs do not introduce an inversion into the crystal, ZB AlGaN may not be formed at the boundaries. Therefore, electron and hole wave functions may overlap well to emit the light, as is the case with the bulk of the epilayer.

Finally, with respect to the deep-state emission bands (B4, B5, and B6), they principally are originating from certain donor-defect companies (DX-type luminescence centers) associated with V_{III}. To assign these bands, we refer to our database for the point defects in GaN,[15,16,35,36] AlN,[37,38] and AlGaN (Refs. 15, 16, 29, and 39) probed using the monoenergetic positron-annihilation technique,[40–42] as well as the literature published by other researchers.[43–45] At first, B6 (marked by pentagons in Figs. 6 and 7) is assigned to originate from V_{III}-O complexes because the yellow luminescence band at 2.2 eV in GaN and the similar CL band at 3.1 eV in AlN have been assigned to originate from Ga vacancy (V_{Ga}^{-})-oxygen complexes (V_{Ga}^{-}-O) and Al vacancy (V_{Al})-oxygen complexes (V_{Al}^{3-}-O), respectively,[36–39,43] and the peak energies are smoothly connected with respect to x in Fig. 7. The origin of B5, which was observed only in the *m*-plane AlN film grown by MOVPE and marked by a descending triangle, is assigned to associate with V_{Al}^{2-}-O or V_{Al}-Si DX center.[37,38,44] Finally, B4 (marked by ascending triangles) may have an analogous origin as the band at 4.6 eV in AlN (Ref. 37): V_{Al} (and V_{Ga}) in $Al_xGa_{1-x}N$ is the major culprit because the formation energy of V_{III}, especially V_{Al}, in $Al_xGa_{1-x}N$ is quite low and even negative for middle-high x.[45] Further reduction in V_{III} concentration by means of high-temperature growth[46] is desirable because certain complexes containing V_{III} have been found to act as major nonradiative recombination centers.[15,16,36,39]

IV. CONCLUSION

The impacts of grown-in anisotropic tilt mosaics of state-of-the-art *m*-plane FS-GaN on the structural and luminescent properties of *m*-plane $Al_xGa_{1-x}N$ epilayers were discussed. The cross-sectional TEM and TED observations revealed that BSF formation was hard to avoid in the case of lattice-mismatched $Al_xGa_{1-x}N$ thick film growth. In addition, the anisotropic greater *m*-plane tilt mosaic along the *a*-axis of FS-GaN, which came from twist mosaics of the original *c*-plane FS-GaN, was shown to give rise to pronounced formations of surface striations along the *c*-axis and PDNs on prismatic $\{10\bar{1}0\}$ planes and pyramidal $\{1\bar{1}0n\}$ planes, even in pseudomorphic $Al_xGa_{1-x}N$ epilayers. These BSFs and planar defects were assigned by SRCL and TRPL measurements to associate with characteristic emission peaks energetically lower than the NBE emission peak. Based on our database for point defects in $Al_xGa_{1-x}N$ alloys, the deep-state CL bands were assigned to originate from cation-vacancy complexes. Further reduction in the structural mosaics of quasi-bulk GaN wafers is necessary to eliminate extra formation of structural and point defects in epitaxial films and quantum structures.

ACKNOWLEDGMENTS

The authors thank K. Fujito, H. Namita, H. Itoh, and K. Shimoyama of Mitsubishi Chemical Holdings for providing *m*-plane FS-GaN. They also thank F. Sato, Y. Murakami, D. Shindo, and M. Terauchi for TEM, TED, and CBED measurements. The authors would like to thank A. Vedono for the discussion on position annihilation spectroscopy. This work was supported in part by Grant-in-Aids of CANTech, IMRAM, Tohoku University, Scientific Research in Priority Area No. 18069001 under MEXT, Japan; NEDO programs by METI, Japan; and AOARD/AFOSR (Grant Nos. FA2386-09-1-4013 and FA2386-10-1-4100) monitored by G. Jessen.

[1] O. Ambacher, B. Foutz, J. Smart, J. R. Shealy, N. G. Weimann, K. Chu, M. Murphy, A. J. Sierakowski, W. J. Schaff, L. F. Eastman, R. Dimitrov, A. Mitchell, and M. Stutzmann, J. Appl. Phys. **87**, 334 (2000).
[2] D. A. Miller, D. S. Chemla, T. C. Damen, A. C. Gossard, W. Wiegmann, T. H. Wood, and C. A. Burrus, Phys. Rev. Lett. **53**, 2173 (1984).
[3] D. A. Miller, D. S. Chemla, T. C. Damen, A. C. Gossard, W. Wiegmann, T. H. Wood, and C. A. Burrus, Phys. Rev. B **32**, 1043 (1985).
[4] P. Waltereit, O. Brandt, A. Trampert, H. T. Grahn, J. Menniger, M. Ramsteiner, M. Reiche, and K. H. Ploog, Nature (London) **406**, 865 (2000).
[5] T. J. Baker, B. A. Haskell, F. Wu, P. T. Fini, J. S. Speck, and S. Nakamura, Jpn. J. Appl. Phys., Part 2 **44**, L920 (2005).
[6] J. S. Speck and S. F. Chichibu, MRS Bull. **34**, 304 (2009), and the papers therein.
[7] T. Takeuchi, H. Amano, and I. Akasaki, Jpn. J. Appl. Phys., Part 1 **39**, 413 (2000).
[8] M. C. Schmidt, K.-C. Kim, H. Sato, N. Fellows, H. Masui, S. Nakamura, S. P. DenBaars, and J. S. Speck, Jpn. J. Appl. Phys., Part 2 **46**, L126 (2007).
[9] K. Okamoto, H. Ohta, S. F. Chichibu, J. Ichihara, and H. Takasu, Jpn. J. Appl. Phys., Part 2 **46**, L187 (2007).
[10] M. C. Schmidt, K.-C. Kim, R. M. Farrell, D. F. Feezell, D. A. Cohen, M. Saito, K. Fujito, J. S. Speck, S. P. DenBaars, and S. Nakamura, Jpn. J. Appl. Phys., Part 2 **46**, L190 (2007).
[11] Y. Enya, Y. Yoshizumi, T. Kyono, K. Akita, M. Ueno, M. Adachi, T. Sumitomo, S. Tokuyama, T. Ikegami, K. Katayama, and T. Nakamura, Appl. Phys. Express **2**, 082101 (2009).
[12] A. Tyagi, R. Farrell, K. Kelchner, C. Huang, P. Hsu, D. Haeger, M. Hardy, C. Holder, K. Fujito, D. Cohen, H. Ohta, J. Speck, S. P. DenBaars, and S. Nakamura, Appl. Phys. Express **3**, 011002 (2010).
[13] K. Fujito, K. Kiyomi, T. Mochizuki, H. Oota, H. Namita, S. Nagao, and I. Fujimura, Phys. Status Solidi A **205**, 1056 (2008).
[14] T. Fujiwara, S. Rajan, S. Keller, M. Higashiwaki, J. Speck, S. P. DenBaars, and U. Mishra, Appl. Phys. Express **2**, 011001 (2009).
[15] S. F. Chichibu, A. Uedono, T. Onuma, B. A. Haskell, A. Chakraborty, T. Koyama, P. T. Fini, S. Keller, S. P. DenBaars, J. S. Speck, U. K. Mishra, S. Nakamura, S. Yamaguchi, S. Kamiyama, H. Amano, I. Akasaki, J. Han, and T. Sota, Nature Mater. **5**, 810 (2006).
[16] S. F. Chichibu, A. Uedono, T. Onuma, B. A. Haskell, A. Chakraborty, T. Koyama, P. T. Fini, S. Keller, S. P. DenBaars, J. S. Speck, U. K. Mishra, S. Nakamura, S. Yamaguchi, S. Kamiyama, H. Amano, I. Akasaki, J. Han, and T. Sota, Philos. Mag. **87**, 2019 (2007).
[17] T. Hoshi, K. Ohshita, M. Kagaya, K. Fujito, H. Namita, K. Hazu, T.

Onuma, and S. F. Chichibu, Appl. Phys. Lett. **94**, 071910 (2009).
[18]S. F. Chichibu, H. Yamaguchi, L. Zhao, M. Kubota, K. Okamoto, and H. Ohta, Appl. Phys. Lett. **92**, 091912 (2008); **93**, 129901 (2008).
[19]R. People and J. C. Bean, Appl. Phys. Lett. **47**, 322 (1985).
[20]T. Onuma, T. Koyama, A. Chakraborty, M. McLaurin, B. A. Haskell, P. T. Fini, S. Keller, S. P. DenBaars, J. S. Speck, S. Nakamura, U. K. Mishra, T. Sota, and S. F. Chichibu, J. Vac. Sci. Technol. B **25**, 1524 (2007).
[21]E. C. Young, C. S. Gallinat, F. Wu, and J. S. Speck, International Workshop on Nitride Semiconductors (IWN), 2008 (unpublished), Paper No. WS2c-P8.
[22]S. F. Chichibu, H. Yamaguchi, L. Zhao, M. Kubota, T. Onuma, K. Okamoto, and H. Ohta, Appl. Phys. Lett. **93**, 151908 (2008).
[23]D. N. Zakharov and Z. Liliental-Weber, Phys. Rev. B **71**, 235334 (2005).
[24]P. Vennéguès, F. Mathal, and Z. Bougrioua, Phys. Status Solidi C **3**, 1658 (2006).
[25]W. Neumann, A. Mogilatenko, T. Wernicke, E. Richter, M. Weyers, and M. Kneissl, J. Microsc. **237**, 308 (2010).
[26]J. E. Northrup, J. Neugebauer, and L. T. Romano, Phys. Rev. Lett. **77**, 103 (1996).
[27]B. A. Haskell, F. Wu, S. Matsuda, M. D. Craven, P. T. Fini, S. P. DenBaars, J. S. Speck, and S. Nakamura, Appl. Phys. Lett. **83**, 1554 (2003).
[28]R. Armitage, M. Horita, J. Suda, and T. Kimoto, J. Appl. Phys. **101**, 033534 (2007).
[29]T. Onuma, S. F. Chichibu, A. Uedono, T. Sota, P. Cantu, T. M. Katona, J. F. Keading, S. Keller, U. K. Mishra, S. Nakamura, and S. P. DenBaars, J. Appl. Phys. **95**, 2495 (2004).
[30]H. Okumura, H. Hamaguchi, T. Koizumi, K. Balakrishnan, Y. Ishida, M. Arita, S. Chichibu, H. Nakanishi, T. Nagatomo, and S. Yoshida, J. Cryst. Growth **189–190**, 390 (1998).
[31]P. P. Paskov, R. Schifano, B. Monemar, T. Paskova, S. Figge, and D. Hommel, J. Appl. Phys. **98**, 093519 (2005).
[32]R. Liu, A. Bell, F. A. Ponce, C. Q. Chen, J. W. Yang, and M. A. Khan, Appl. Phys. Lett. **86**, 021908 (2005).
[33]R. Kröger, T. Paskova, and A. Rosenauer, Springer Proc. Phys. **120**, 49 (2007).
[34]P. Corfdir, P. Lefebvre, J. Levrat, A. Dussaigne, J.-D. Ganière, D. Martin, J. Ristić, T. Zhu, N. Grandjean, and B. Deveaud-Plédran, J. Appl. Phys. **105**, 043102 (2009).
[35]A. Uedono, S. F. Chichibu, Z. Q. Chen, M. Sumiya, R. Suzuki, T. Ohdaira, T. Mikado, T. Mukai, and S. Nakamura, J. Appl. Phys. **90**, 181 (2001).
[36]S. F. Chichibu, A. Uedono, T. Onuma, T. Sota, B. A. Haskell, S. P. DenBaars, J. S. Speck, and S. Nakamura, Appl. Phys. Lett. **86**, 021914 (2005).
[37]T. Koyama, M. Sugawara, T. Hoshi, A. Uedono, J. F. Kaeding, R. Shama, S. Nakamura, and S. F. Chichibu, Appl. Phys. Lett. **90**, 241914 (2007).
[38]A. Uedono, S. Ishibashi, S. Keller, C. Moe, P. Cantu, T. M. Katona, D. S. Kamber, Y. Wu, E. Letts, S. A. Newman, S. Nakamura, J. S. Speck, U. K. Mishra, S. P. DenBaars, T. Onuma, and S. F. Chichibu, J. Appl. Phys. **105**, 054501 (2009).
[39]S. F. Chichibu, A. Uedono, T. Onuma, S. P. DenBaars, U. K. Mishra, J. S. Speck, and S. Nakamura, Mater. Sci. Forum **590**, 233 (2008).
[40]R. Krause-Rehberg and H. S. Leipner, *Positron Annihilation in Semiconductors*, Solid-State Sciences (Springer, Berlin, 1999), Vol. 127, pp. 5–47.
[41]P. G. Coleman, *Positron Beams and Their Application* (World Scientific, Singapore, 2000), pp. 11–40.
[42]A. van Veen, H. Schut, M. Clement, J. M. M. de Nijs, A. Kruseman, and M. R. IJpma, Appl. Surf. Sci. **85**, 216 (1995).
[43]J. Neugebauer and C. G. Van de Walle, Appl. Phys. Lett. **69**, 503 (1996).
[44]A. Dadgar, A. Krost, J. Christen, B. Bastek, F. Bertram, A. Krtschil, T. Hempel, J. Blasing, U. Haboeck, and A. Hoffmann, J. Cryst. Growth **297**, 306 (2006).
[45]C. Stampfl and C. G. Van de Walle, Appl. Phys. Lett. **72**, 459 (1998).
[46]S. F. Chichibu, T. Onuma, K. Hazu, and A. Uedono, Appl. Phys. Lett. **97**, 201904 (2010).

(3) MOVPE and characterization of *m*-plane $Al_{1-x}In_xN$ films on the freestanding GaN substrates

Abstract

Epitaxial growth and characterizations were carried out on *m*-plane AlInN alloys. In order to eliminate the polarization discontinuity at the barrier/channel interface to obtain normally-off (*E*-mode) HFETs, the use of an AlInN barrier lattice-matched to GaN is one of the best solutions. As a preliminary result, we succeeded in growing epitaxial *m*-plane $Al_{1-x}In_xN$ alloys on the MCC *m*-plane FS-GaN substrates, and observed UV luminescence peaks ranging from 214 to 400 nm at room temperature.

Anisotropic lattice-mismatch of *m*-plane AlInN on GaN

Calculated strain values of *m*-plane $Al_{1-x}In_xN$ films coherently grown on *m*-plane GaN are shown as a function of InN mole fraction, *x*, in Fig. 3-1. As shown, the films of particular *x* may have little strain. For example, the *a*-lattice parameter of $Al_{0.83}In_{0.17}N$ matches to that of GaN and the *c*-lattice parameter of $Al_{0.74}In_{0.26}N$ matches to GaN along the *c*-axis. Therefore, epitaxial growths of *m*-plane $Al_{1-x}In_xN$ (*x* close to 0.2) on GaN will make a sense to fabricate coherent *m*-plane heterostructures. For example, BSF density for the *c*-lattice-matched $Al_{0.74}In_{0.26}N$ is expected to be lower than that for the films of other InN mole fractions. As the bandgap energy of $Al_{0.83}In_{0.17}N$ is expected to be higher than that of GaN, $Al_{0.83}In_{0.17}N$/GaN structure can be expected to be a basic structure for *E*-mode HFETs. Indeed, reduced strain might prevent the alloy films from cracking and from introducing BSFs and PSFs, resulting in reduced scattering of 2DEG by those structural defects.

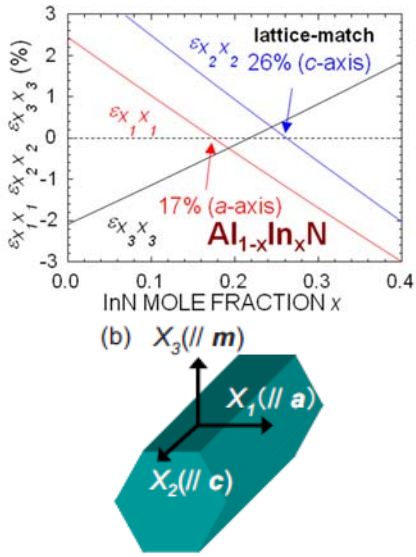

Fig. 3-1 Calculated strain values and the definition of three axes for *m*-plane $Al_{1-x}In_xN$ on a FS-GaN substrate.

Growth conditions

All the *m*-plane AlInN epilayers were grown by MOVPE. The MCC *m*-plane FS-GaN substrates[1] were confirmed by the TEM observation to have TDs lower than 5×10^6 cm^{-2} and BSFs lower than 10^3 cm^{-1}. After growing 1-μm-thick *m*-plane GaN using trimethylgallium (TMGa) and ammonia (NH_3),[2] *m*-plane $Al_{1-x}In_xN$ alloy films were grown using trimethylaluminium (TMAl), trimethylindium (TMIn), and NH_3. The reactor pressure, V/III ratio, and growth temperature (T_g) were $2.0\sim4.0\times10^4$ Pa, 62000~100000, and 630~870°C, respectively. Approximately 500~600-nm-thick films were grown at the rate (R_g) approximately 0.28 μm/h.

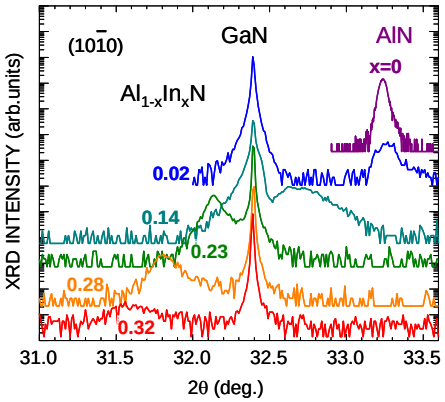

Fig. 3-2 The 2θ-ω XRD patterns for the *m*-plane $Al_{1-x}In_xN$ films on the MCC *m*-plane FS-GaN.

Results and discussion

The surface of very thin, coherent *m*-plane $Al_{1-x}In_xN$ films exhibited pretty smooth morphology. However,

once the thickness exceeds the critical one, the morphology exhibited segmented rectangles, due presumably to the in-plane biaxial anisotropic lattice-mismatch.

The 2θ-ω XRD patterns for the (10-10) diffraction of the *m*-plane $Al_{1-x}In_xN$ films are shown in Fig. 3-2. The diffraction peak can be seen for all the epilayers (x=0 to 0.32), and the diffraction angle decreased continuously as x increases.

The films of $0.17 \leq x \leq 0.32$ were confirmed by the x-ray reciprocal space mapping (X-RSM) method to be mostly coherently grown on GaN. However, the films for $x<0.14$ were essentially tensile strained, and most of the films were relaxed due to cracking. The measured strain values are shown in Fig. 3-3. The importance of lattice-matching is also visualized by measuring the FWHM values for the x-ray rocking curves (XRCs). Both the tilt and twist mosaics of the films showed the smallest FWHM values around 100 arcsec for $0.26 \leq x \leq 0.28$. The result means that lattice-matched and compressively-strained films have lower density TDs.

Steady-state CL spectra of the *m*-plane $Al_{1-x}In_xN$ films are shown in Fig. 3-4. The peak energy and wavelength for the NBE emission of *m*-plane AlN were 5.80 eV and 214 nm, respectively. As x increases, the emission color changed from UV to green.

Their low temperature luminescence spectra and carrier recombination dynamics will be investigated in the future.

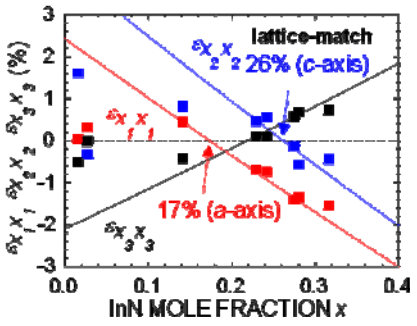

Fig. 3-3 Measured strain values for the *m*-plane $Al_{1-x}In_xN$ films grown on FS-GaN substrates.

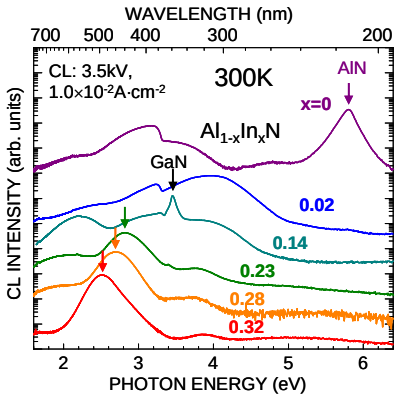

Fig. 3-4 Room temperature CL spectra for the *m*-plane $Al_{1-x}In_xN$ films grown on FS-GaN substrates.

References

1) K. Fujito, K. Kiyomi, T. Mochizuki, H. Oota, H. Namita, S. Nagao, and I. Fujimura, Phys. Status Solidi A 205, 1056 (2008).
2) S. F. Chichibu, H. Yamaguchi, L. Zhao, M. Kubota, K. Okamoto, and H. Ohta, Appl. Phys. Lett. 92, 091912 (2008); Erratum *ibid*. 93, 129901 (2008).

(4) MOVPE and characterization of AlGaN / GaN and AlInN / GaN heterostructures

Abstract

Heterostructures of AlGaN/GaN and AlInN/GaN were grown by MOVPE on the MCC *m*-plane FS-GaN substrates. As far as the barrier layers were thin enough, the surface exhibited smooth morphology with monolayer atomic step lines. We finally asked AFRL to process the wafers. However, because the substrate was semi-conducting, we were not able to electrically isolate them from the channel, so all the HFET structures exhibited leaky *I-V* characteristics and we did not see clear indication of 2DEG conduction at room temperature.

Growth of the heterostructures

Heterostructures of *m*-plane Si-doped $Al_{0.2}Ga_{0.8}N$/GaN and Si-doped $Al_{0.82}In_{0.18}N$/GaN were grown by MOVPE on the MCC *m*-plane FS-GaN substrates. The surface AFM images of them are shown in Fig. 4-1 and 4-2, respectively. The surface of $Al_{0.2}Ga_{0.8}N$/GaN exhibited a fairly smooth morphology with monolayer atomic step lines. However, it contained large-scale hillocks that originate from the substrate itself. On the other hand, the surface of $Al_{0.82}In_{0.18}N$/GaN was characterized by deep crevasses aligned almost normal to the *c*-axis. It might originate from the substrate or underlayer GaN. These results imply that *m*-plane FS-GaN quality is not yet stabilized.

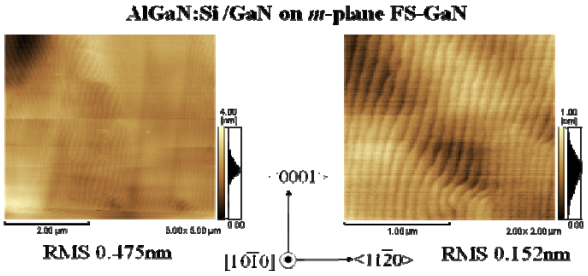

Fig. 4-1 Surface AFM image of the *m*-plane $Al_{0.2}Ga_{0.8}N$ / GaN heterostructure capped by an 1-nm-thick GaN.

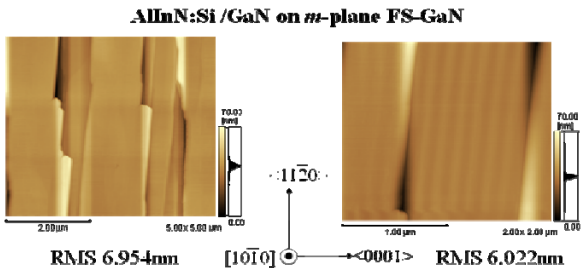

Fig. 4-2 Surface AFM image of the *m*-plane $Al_{0.82}In_{0.18}N$ / GaN heterostructure capped by an 1-nm-thick GaN.

Because it was not able to completely isolate the semiconducting FS-GaN substrates, we were not able to see clear indication of 2DEG conduction at room temperature and the HFET structures exhibited leaky *I-V* curves. We must deposit semi-insulating layer or even AlGaN or AlN isolation layer to see the channels.

Throughout this study, however, we obtained basic knowledge on the polarization characteristics and strain configurations of *m*-plane AlGaN and AlInN films on FS-GaN suffering from anisotropic stresses.

Following is the list of the papers and the presentation at Int'l confs.

Paper

1. K. Hazu, M. Kagaya, T. Hoshi, T. Onuma, and S. F. Chichibu, "Impacts of anisotropic tilt mosaics of state-of-the-art *m*-plane freestanding GaN substrates on the structural and luminescent properties of *m*-plane $Al_xGa_{1-x}N$ epilayers", Journal of Vacuum Science and Technology B 29 (2), pp.021208 1-9 (2011).
2. K. Hazu and S. F. Chichibu, "Optical polarization properties of *m*-plane $Al_xGa_{1-x}N$ epitaxial films grown on *m*-plane freestanding GaN substrates toward nonpolar ultraviolet LEDs", Optics Express 19 (S4), pp.A1008-A1021 (2011).

Presentation

1. K. Hazu, M. Kagaya, T. Hoshi, T. Onuma, and S. F. Chichibu, "Identification of cathodoluminescence peaks in *m*-plane $Al_xGa_{1-x}N$ epilayers grown on freestanding GaN substrates prepared by halide vapor phase epitaxy", The Third International Symposium on Growth of III-Nitrides (ISGN-3), Montpellier, France, Jul. 4-7 (2010), No.TU2-5 (oral).